Marine Pollution Bulletin 222 (2026) 118713

Contents lists available at ScienceDirect

Marine Pollution Bulletin

journal homepage: www.elsevier.com/locate/marpolbul

Current contamination trends and historical records of traditional and emerging polycyclic aromatic hydrocarbons in sediments from Yeongil Bay and Hupo Region, East Sea

Jihyun Cha [a,1], Chang-Eon Lee [b,c,1], Mungi Kim [a], Youngnam Kim [c], Jiyun Gwak [c], Dong Jin Joe [a], Jae-Hyun Lim [d], In Kwon Um [e], Man Sik Choi [a,c], Seongjin Hong [a,c,*]

[a] Department of Marine Environmental Sciences & Institute of Marine Environmental Sciences, Chungnam National University, Daejeon, 34134, Republic of Korea
[b] Marine Environment Research Department, Korea Institute of Ocean Science and Technology, Busan, 49111, Republic of Korea
[c] Department of Earth, Environmental & Space Sciences, Chungnam National University, Daejeon, 34134, Republic of Korea
[d] Marine Environmental Research Division, National Institute of Fisheries Science, Busan, 46083, Republic of Korea
[e] Petroleum and Marine Research Division, Korea Institute of Geoscience and Mineral Resources, Daejeon, 34132, Republic of Korea

ARTICLE INFO

Keywords:
Polycyclic aromatic hydrocarbons
Sediment
PMF modeling
Coal combustion
Hazard quotient
East Sea

ABSTRACT

This study investigated the distribution, potential sources, and ecological risks of traditional and emerging polycyclic aromatic hydrocarbons (t-PAHs and e-PAHs) in sediments from Yeongil Bay ($n = 17$), the Hupo Basin ($n = 20$), and the Hupo Bank ($n = 6$) in the East Sea of Korea. Sediment properties were characterized using carbon and nitrogen stable isotope ratios, grain size, total organic carbon (TOC), and total nitrogen (TN) contents. Concentrations of 15 t-PAHs and 8 e-PAHs were significantly higher in Yeongil Bay (490 ng g^{-1} dm), while similar levels were found in the Hupo Basin (160 ng g^{-1} dm) and the Hupo Bank (96 ng g^{-1} dm). Multivariate analysis revealed that these regions were primarily distinguished by TN, TOC, and 3-ring PAHs. Positive matrix factorization identified vehicle emissions, coal combustion, and steel production as the main sources of PAHs in Yeongil Bay. In the Hupo region, vehicle emissions, biomass combustion, and coal combustion were the dominant sources, with coal combustion being the most influential in the Hupo Basin and vehicle emissions in the Hupo Bank. Hazard quotient analysis indicated that benzo[*g,h,i*]perylene and indeno[*1,2,3-cd*]pyrene were the primary contributors to ecological risk. Temporal trends in core sediments from the Hupo Basin revealed a continuous presence of PAHs since the pre-industrial period, with either long-term persistence or recent increases across different cores. This study provides insights into the spatiotemporal distribution and environmental behavior of PAHs, offering a scientific basis for environmental monitoring and management.

1. Introduction

Polycyclic aromatic hydrocarbons (PAHs) are hydrophobic organic pollutants primarily generated during the incomplete combustion of fossil fuels, vehicle exhaust, and biomass (Ravindra et al., 2008). Due to their persistence and capacity for long-range atmospheric and oceanic transport, PAHs are widely distributed across various environmental compartments, including air, water, soil, and sediments (Balmer et al., 2019). Their bioaccumulative potential and toxicity to organisms have led the U.S. Environmental Protection Agency (EPA) to designate 16 PAHs as priority pollutants (Neff, 1979). In recent years, interest has expanded beyond these 16 traditional PAHs (t-PAHs) to include emerging PAHs (e-PAHs), which share similar sources, environmental fate, and toxicological profiles (Cha et al., 2019; Kim et al., 2019).

PAHs released from both point and non-point sources can eventually be transported to the marine environment (Kim et al., 2021). Due to their strong adsorption capacity and physicochemical stability, PAHs can persist in sediments for extended periods (Maletić et al., 2019). These compounds may pose ecological risks by entering benthic food webs and affecting sediment-dwelling organisms (Wang et al., 2025). Marine sediments, therefore, serve as major reservoirs and long-term secondary sources of PAHs, making them a critical matrix for coastal

* Corresponding author at: Department of Marine Environmental Sciences & Institute of Marine Environmental Sciences, Chungnam National University, Daejeon, 34134, Republic of Korea.
E-mail address: hongseongjin@cnu.ac.kr (S. Hong).
[1] These authors contributed equally to this work.

https://doi.org/10.1016/j.marpolbul.2025.118713
Received 8 July 2025; Received in revised form 13 August 2025; Accepted 11 September 2025

ecosystem monitoring (Lee et al., 2022; Skotvold and Savinov, 2003). In particular, core sediments act as environmental archives, preserving chronological records of contaminant accumulation (Liu et al., 2012; Yoon et al., 2025). Core sediments with established chronological frameworks, typically determined using radionuclides such as ^{210}Pb, are especially useful for quantitatively assessing the spatiotemporal distribution and fluxes of PAHs (Liu et al., 2012).

The distribution of PAHs in marine sediments is influenced not only by their sources but also by environmental factors such as total organic carbon (TOC) content, grain size, and sedimentation patterns and rates (Zhao et al., 2020). Moreover, the physicochemical properties of PAHs play a critical role in determining their environmental transport and fate (Cha et al., 2024). Given these complexities, multivariate statistical methods such as partial least squares (PLS) and principal component

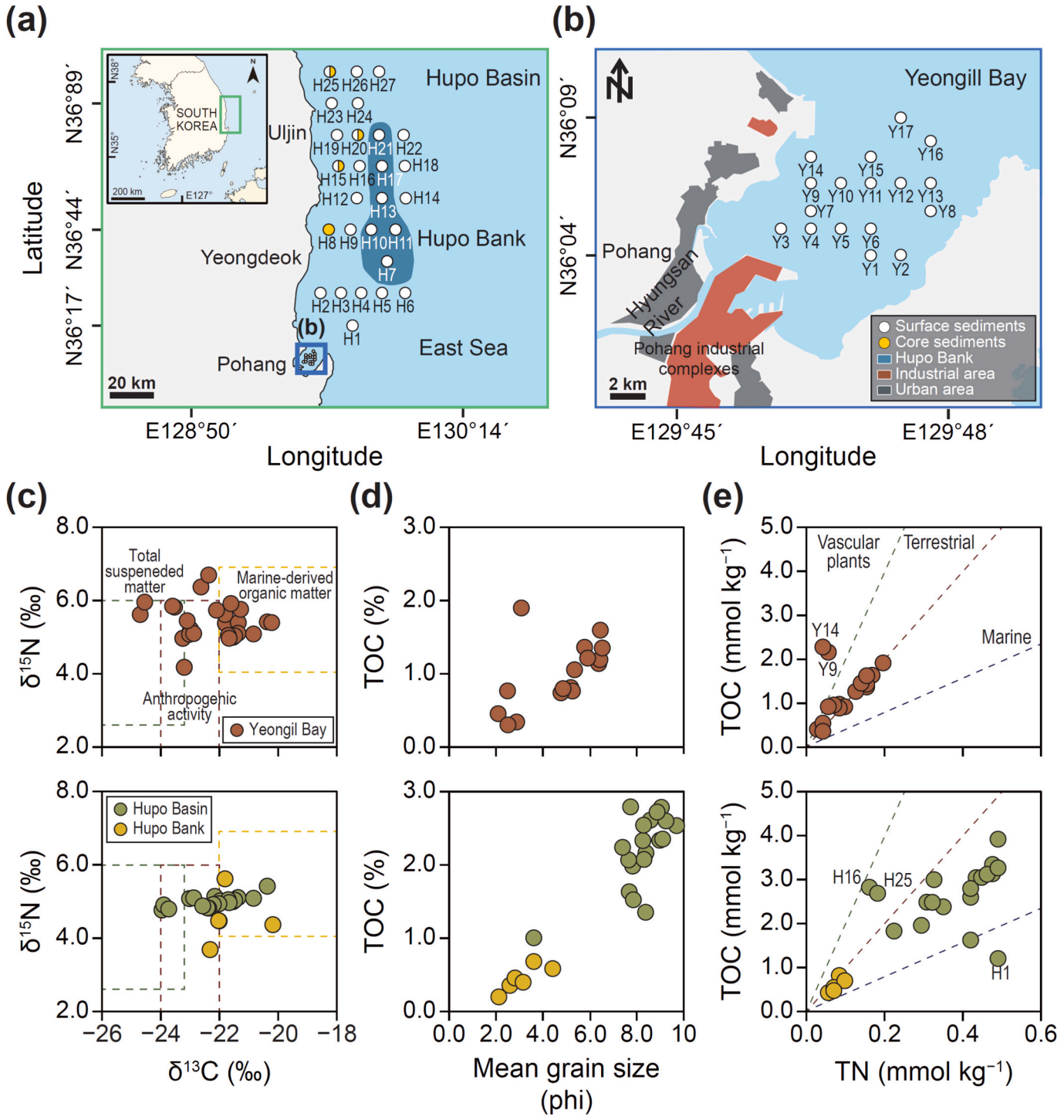

Fig. 1. (a) Map showing surface and core sediment sampling sites in Yeongil Bay, the Hupo Basin, and the Hupo Bank, East Sea. (b) Enlarged map of the Yeongil Bay region. White circles denote surface sediment sampling sites, and yellow circles represent core sediment sites. (c) Distribution of δ^{13}C (‰) and δ^{15}N (‰) values in surface sediments [potential sources as reported by Wu et al., 2007]. (d) Relationship between mean grain size (phi) and total organic carbon contents (TOC, %). (e) Relationship between TOC (%) and total nitrogen (TN, %) in sediments. (For interpretation of the references to colour in this figure legend, the reader is referred to the web version of this article.)

analysis (PCA) have been applied to distinguish spatial patterns in PAHs distribution (Mali et al., 2022). Unlike many industrial pollutants, PAHs are not intentionally produced but are instead formed unintentionally through various combustion processes, with some contributions from natural sources (Na et al., 2021; Wilcke, 2007). To identify these diverse sources, receptor models such as positive matrix factorization (PMF) are widely used for quantitative source apportionment (Yang et al., 2021).

Yeongil Bay is located in Pohang, a major industrial port city on the southeastern coast of Korea, where industries such as steel production, shipbuilding, and petrochemical manufacturing are concentrated (Gwak et al., 2022). Environmental pollutants, including PAHs, are primarily introduced into the bay via the Hyeongsan River, and the area has been reported as a site of ongoing marine pollution (An et al., 2021; Gwak et al., 2022; Hong et al., 2014b). A previous study also found that mercury from the Hyeongsan River was transported to coastal areas as far north as approximately 36.6°N (Joe et al., 2022). The Hupo Basin is a less industrialized coastal region of the East Sea (35°N–40°N), where water circulation and sediment transport are influenced by the convergence of the East Korea Warm Current and the North Korea Cold Current (Hong et al., 2022a). The Hupo Bank, a geomorphological uplift, lies parallel to the coastline between Uljin and Yeongdeok, while the adjacent Hupo Basin is a subsiding depression formed by tectonic extension and subsequent compression associated with the opening of the East Sea (Park et al., 2022).

The main objective of this study was to investigate the distribution patterns, potential sources, and ecological risks of PAHs in sediments from Yeongil Bay and the Hupo region in the East Sea of Korea. To this end, we analyzed carbon and nitrogen stable isotope ratios, grain size, TOC, and total nitrogen (TN) in the sediments, and assessed the spatial distribution of 23 PAHs (15 t-PAHs and 8 e-PAHs). Multivariate statistical techniques were used to identify key environmental factors and spatial patterns, and PMF modeling was applied to estimate potential sources of PAHs. Ecological risks were evaluated using a hazard quotient (HQ)-based analysis. Vertical distribution patterns, source changes, and anthropogenic PAH fluxes were further examined using sediment core data. This study provides an integrated understanding of the long-term fate, source apportionment, and ecological risks of PAHs in sediments of the East Sea, a region influenced by overlapping industrial, urban, and marine activities.

2. Materials and methods

2.1. Sample collection and preparation

Surface and core sediments were collected in 2014 and 2017 aboard the R/V *Tamhae-II*, operated by the Korea Institute of Geoscience and Mineral Resources (Fig. 1a and b). Details of the sampling sites are provided in Tables S1 and S2 of the Supplementary Materials. The sampling procedures for both surface and core sediments have been described previously (Joe et al., 2022). Briefly, surface sediments were obtained from 43 sites across Yeongil Bay ($n = 17$), the Hupo Basin ($n = 20$), and the Hupo Bank ($n = 6$) using a box corer. In addition, core sediments were collected at four sites in the Hupo Basin using 40 cm-long acrylic tubes inserted into the box corer. Each core was sectioned as follows: the top 1.0 cm was sampled separately, followed by slices of 2.0 cm, 3.0 cm, 4.0 cm, and 5.0 cm thickness from the 0–10 cm, 10–20 cm, 20–30 cm, and > 30 cm layers, respectively. Sediment sections were collected with a plastic scoop, weighed to determine moisture content, and oven-dried. The dried sediments were homogenized using an agate mortar and stored in sealed containers until analysis.

2.2. Analysis of grain size, TOC, TN, and carbon and nitrogen stable isotope ratios

The method for grain size analysis has been described in detail in a previous study (Joe et al., 2022). Briefly, grain size was measured using a laser scattering particle size analyzer (Microtrac S3500, Pennsylvania) after the removal of carbonates and organic matter. For TOC analysis, 8 mL of 1 M hydrochloric acid was added to each sediment sample (~1 g) to eliminate inorganic carbon prior to measurement. TN was analyzed without pretreatment. TOC and TN contents, along with their stable isotope compositions, were determined using an elemental analyzer (EA) coupled to an isotope ratio mass spectrometer (IRMS; Isoprime 100, GV Instruments, Manchester, UK). The stable isotope ratios of carbon and nitrogen ($\delta^{13}C$ and $\delta^{15}N$) in sedimentary organic matter were analyzed following previously established methods (Logan and Lutcavage, 2008; Lorrain et al., 2015). Isotopic values of TOC and TN were expressed in delta (δ) notation relative to the Vienna Pee Dee Belemnite (VPDB) standard for $\delta^{13}C$ and atmospheric nitrogen for $\delta^{15}N$.

2.3. Analysis of PAHs in sediments

A total of 15 t-PAHs and 8 e-PAHs were analyzed in the sediments. The 23 PAH standards were purchased from ChemService (West Chester, PA) and Sigma-Aldrich (St. Louis, MO). The e-PAHs were compounds previously identified in sediments from industrial areas (Kim et al., 2019). Among these, benzo[*b*]naphtho[*2,3-d*]furan, 11H-benzo[*b*]fluorene, benzo[*b*]naphtho[*2,1-d*]thiophene, and 5-methylbenz[*a*]anthracene (5MbA) have been reported to bind to the aryl hydrocarbon receptor (Kim et al., 2019). In addition, quantitative structure-activity relationship-based toxicity predictions indicated that these e-PAHs may exert potential toxic effects, including carcinogenicity, mutagenicity, and developmental toxicity (An et al., 2020). For the analysis of PAHs in sediments, two extraction methods were used: Soxhlet extraction and accelerated solvent extraction (ASE, Dionex ASE 350, Thermo Scientific, Salt Lake, UT). Soxhlet extraction was applied to surface sediments from Yeongil Bay and the Hupo Basin, while ASE was used for core sediment samples from the Hupo Basin. For Soxhlet extraction, approximately 5.0 g of freeze-dried sediment was mixed with anhydrous sodium sulfate in a cellulose thimble, followed by extraction with methylene chloride (MC, Honeywell, Charlotte, NC) for 16 h. For ASE, 5.0 g of dried sediment was loaded into a 34 mL stainless steel cell and extracted at 120 °C for 10 min using MC. For both methods, surrogate PAH standards (acenaphthene-d10, phenanthrene-d10, chrysene-d12, and perylene-d12) were spiked into each sample at 100 ng prior to extraction. The organic extracts were concentrated to 1.0 mL using a rotary evaporator, followed by a nitrogen blowdown. Elemental sulfur and organic sulfur compounds in sediment extracts can interfere with PAHs analysis by reducing peak resolution, increasing baseline noise, and decreasing sensitivity. To remove these interferences, activated copper (Sigma-Aldrich) was added to the extracts (Smith et al., 1984). Purification was carried out using silica gel column chromatography (8 g). Compounds were separated by polarity: the non-polar fraction (F1) was eluted with 30 mL of hexane, and the mid-polar fraction (F2) was eluted with a hexane:MC (8:2, *v*/v) mixture. The F2 fraction was used for PAH analysis. The eluent was concentrated to 1.0 mL, transferred to a GC vial (Agilent Technologies, Santa Clara, CA), and spiked with an internal standard (2-fluorobiphenyl). Instrumental analysis was conducted using a gas chromatograph coupled with a mass selective detector (7890B GC and 5977B MSD, Agilent Technologies). A chromatogram of the 23 PAHs is provided in Fig. S1. To verify the performance and quantification accuracy of the analytical method, validation using NIST SRM 1944 yielded satisfactory PAHs recoveries ranging from 45% to 104% (mean = 75%). The limit of detection (LOD) and quantification (LOQ) were calculated by multiplying the standard deviation of the lowest calibration standards by 3.143 and 10, respectively. The recovery rates of Soxhlet and ASE extractions were found to be comparable. Detailed information on target PAHs, retention times, LOD, LOQ, recoveries, and instrumental conditions is provided in Tables S3 and S4.

2.4. Multivariate analysis and PMF modeling

To investigate the spatial distribution characteristics of PAHs in sediments, multivariate statistical techniques, such as PLS and PCA, were applied. PLS and PCA were performed using R software (version 4.2.3) to visualize inter-sample patterns and identify key variables contributing to regional differentiation. All datasets were $\log_{10}$-transformed after adding 1.0 to avoid undefined values due to zeros, followed by *Z*-score normalization to standardize variables and eliminate unit-based differences. PCA was conducted using the prcomp function, while PLS-discriminant analysis (DA) was performed with the opls function from the "ropls" R package. The suitability of the dataset for PCA was assessed using Bartlett's test of sphericity and the Kaiser-Meyer-Olkin (KMO) measure. A KMO value above 0.6 indicates adequacy for PCA. PLS-DA model performance was evaluated using cumulative goodness-of-fit (R^2Y), cross-validated predictability (Q^2Y), and permutation tests. A Q^2Y value above 0.3–0.5 is generally considered indicative of a predictive model, and a permutation test *p*-value below 0.05 suggests statistically significant group separation. In this study, the PLS-DA model with two predictive components yielded $R^2Y = 0.531$ and $Q^2Y = 0.447$, with statistical significance confirmed by the permutation test ($p < 0.05$). For statistical analysis, compound concentrations below the LOD were replaced with LOD/2. To identify potential PAH sources, we applied the U.S. EPA's PMF model (Version 5.0). PMF is a multivariate receptor model that decomposes environmental datasets into source profiles and contributions using a least-squares algorithm (Moon et al., 2008). In this study, 15 t-PAHs were used as input. The model was applied separately to sediment datasets from Yeongil Bay and the Hupo region. The optimal number of factors was determined by minimizing the Q-value ratio (Q_{True}/Q_{Exp}), with a three-factor solution providing the best fit. The model was iterated 100 times to ensure convergence. Linear regression between observed and predicted concentrations yielded a coefficient determination (R^2) of 0.99, indicating strong model performance.

2.5. Potential ecological risk assessment

The HQ approach was applied to evaluate the potential ecological risks of PAHs in surface sediments. The calculation method follows a previously published study (Kim et al., 2025). HQ was calculated using Eq. (1), based on the measured environmental concentration (MEC) and the predicted no-effect concentration (PNEC) of each compound:

$$HQ = \frac{MEC}{PNEC_{sediment}} \tag{1}$$

Due to the limited availability of experimental toxicity data for PAHs, PNEC values were estimated using the predicted 50% effective concentration (EC_{50}) from the ECOSAR model (Table S5). These values represent the 96-h growth inhibition concentration for green algae and reflect the toxicity of dissolved or particle-bound PAHs in the water column. To better represent sediment conditions, an equilibrium partitioning approach was used to convert water-based toxicity values into sediment-based PNECs (Li et al., 2016), using Eqs. (2)–(4):

$$K_{susp-water} = F_{water,susp} + F_{solid,susp} \times \frac{F_{oc,susp} \times K_{oc}}{1000} \times \rho_{solid} \tag{2}$$

$$PNEC_{water} = \frac{L(E)C50}{AF} \tag{3}$$

$$PNEC_{sediement} = \frac{K_{susp-water}}{\rho_{susp}} \times PNEC_{water} \times 1000 \tag{4}$$

The suspended soil-water partition coefficient ($K_{sup\text{-}water}$) was calculated based on the following parameters: the volumetric fraction of water and solids in suspended matter ($F_{water,susp} = 0.9\ m^3\ m^{-3}$; $F_{solid,susp} = 0.1\ m^3\ m^{-3}$), the organic carbon content of suspended solids ($F_{oc,susp} = 0.1\ kg\ kg^{-1}$), and the organic carbon-water partition coefficient (K_{OC} in $L\ kg^{-1}$) (Gao et al., 2019). The density of the solid phase (ρ_{solid}) was set at 2500 kg m^{-3}, and the density of suspended solids (ρ_{solid}) at 1150 g L^{-1}. An assessment factor of 1000 was applied to ensure a conservative ecological risk evaluation. Based on the calculated HQ values, ecological risk levels were classified as follows: HQ < 0.1 indicated negligible risk, values between 0.1 and 1.0 were considered to represent low to moderate risk, and HQ ≥ 1.0 indicates potential ecological risk (Lemly, 1996).

In addition, to evaluate the potential carcinogenic and mutagenic toxicities of PAHs in the sediments, benzo[*a*]pyrene (BaP)-equivalent concentrations were calculated. BaP-TEQ (carcinogenic equivalents) and BaP-MEQ (mutagenic equivalents) were determined using Eqs. (5) and (6), respectively. For each PAH congener, its concentration was multiplied by the corresponding toxic equivalence factor (TEF) or mutagenic equivalence factor (MEF). The TEF values (EPA, 1993; Nisbet and Lagoy, 1992) and MEF values (Durant et al., 1996, 1999) were obtained from previously published studies (Table S6).

$$BaP - TEQ = TEF_i \times PAH_i \tag{5}$$

$$BaP - MEQ = MEF_i \times PAH_i \tag{6}$$

2.6. Sediment core dating and calculation of anthropogenic fluxes

Sedimentation rates of core sediments from the Hupo Basin were determined based on a previous study (Joe et al., 2022). Specifically, the constant rate of supply model was applied using excess ^{210}Pb activity in each sediment layer. The average sedimentation rates at sites H8, H15, H20, and H25 were 0.16, 0.45, 0.31, and 0.50 cm y^{-1}, respectively (Table S2). Based on these rates, anthropogenic PAHs fluxes were calculated using Eq. (7):

$$PAHs\ flux\ \left(ng\ m^{-2}\ y^{-1}\right) = PAH\ concentration \times SR \times \rho_{dry} \tag{7}$$

Here, SR is the sedimentation rate (cm y^{-1}), and ρ_{dry} is the bulk density (g cm^{-3}). The anthropogenic flux of PAHs represents the mass of pollutants deposited per unit area and time, calculated from sediment concentrations and accumulation rates. This metric is widely used to quantify the contribution of pollution sources (Li et al., 2023). The calculated fluxes were categorized into three periods (1940–75, 1975–95, 1995–present) based on temporal boundaries established from historical mercury concentration trends in a previous study (Joe et al., 2022).

3. Results and discussion

3.1. Sediment and organic matter properties

Carbon and nitrogen stable isotope ratios, mean grain size, TOC, TN, and C/N ratios were analyzed in sediments from Yeongil Bay, the Hupo Basin, and the Hupo Bank (Table S1). $\delta^{13}C$ and $\delta^{15}N$ values showed spatial variation across the three regions (Fig. 1c). Yeongil Bay and the Hupo Basin exhibited broader ranges, indicating mixed inputs from both marine and terrestrial organic matter, whereas the Hupo Bank showed the most marine-like $\delta^{13}C$ and $\delta^{15}N$ signatures (Wu et al., 2007). In Yeongil Bay, these patterns likely reflect combined inputs from terrestrial runoff associated with industrial and urban activities, riverine discharge, and deposition of suspended particulates. Similarly, the wide range of $\delta^{13}C$ values in the Hupo Basin, along with the proximity of several sites to anthropogenic influences, suggests localized human impact and organic matter mixing driven by coastal hydrodynamic processes.

Grain size and TOC content also differed distinctly among the three regions (Fig. 1d). The mean grain size was smallest in the Hupo Basin (8.2 phi), followed by Yeongil Bay (4.7 phi), and largest in the Hupo Bank (3.1 phi). Sediments from the Hupo Basin were dominated by fine,

clay-like particles, while those from Hupo Bank consisted mainly of very fine sands. TOC content was highest in the Hupo Basin (2.2%), moderate in Yeongil Bay (1.0%), and lowest in the Hupo Bank (0.45%) (Fig. S2). The low TOC in the Hupo Bank may reflect its shallow depth and elevated topography, which result in stronger hydrodynamic conditions that limit organic matter deposition (Kim and Park, 2014). TN content followed a similar pattern, with the highest average TN observed in the Hupo Basin (0.27%), followed by Yeongil Bay (0.07%) and the Hupo Bank (0.05%). C/N ratios further supported the observed differences in organic matter sources. Most sediments from Yeongil Bay, except for Y9 and Y14, exhibited terrestrial signatures (Fig. 1e). In contrast, sediments from the Hupo Basin and Hupo Bank were predominantly marine in origin. Overall, surface sediments from the three regions exhibited distinct geochemical characteristics in terms of organic matter sources and biogeochemical properties, as reflected in stable isotope ratios, TOC, TN, and C/N ratios. These patterns underscore differences in sedimentation processes and organic matter accumulation pathways among the study areas.

3.2. Concentrations and compositions of PAHs in surface sediments

The concentrations of t-PAHs in surface sediments were 460 ng g^{-1} dry mass (dm) in Yeongil Bay, 150 ng g^{-1} dm in the Hupo Basin, and 86 ng g^{-1} dm in the Hupo Bank (Fig. 2a). In Yeongil Bay, the highest concentration was recorded at Y13 (2000 ng g^{-1} dm), followed by Y8 and Y5 (both at 1000 ng g^{-1} dm). Relatively high concentrations of PAHs were observed at H5 (450 ng g^{-1} dm) and H25 (340 ng g^{-1} dm) in the Hupo Basin, exceeding those at several sites of Yeongil Bay. Among the t-PAHs, phenanthrene (Phe, 25 ng g^{-1} dm) showed relatively high concentrations (Table S7), a pattern consistent with findings in both domestic industrial regions and other global studies (An et al., 2020; Gwak et al., 2024; Hong et al., 2022b). This trend is likely due to its origin from both natural and anthropogenic sources, its high emission rates, and physicochemical properties that promote environmental persistence and mobility (Verbruggen and Van Herwijnen, 2012). The concentrations of e-PAHs in Yeongil Bay, the Hupo Basin, and the Hupo Bank were 34, 11, and 9.4 ng g^{-1} dm, respectively (Fig. 2b). Overall, total PAH concentrations in surface sediments were significantly higher in Yeongil Bay compared to the other regions (Fig. 2c).

The spatial distribution of PAHs in surface sediments revealed site-specific hotspots, reflecting spatial variability across the study area (Fig. S3). Among the e-PAHs, 5MbA and benzo[*e*]pyrene (BeP) were found at relatively high concentrations. These two compounds have previously been reported to exhibit potential carcinogenicity in organisms (Villemin et al., 1994). 5MbA is typically associated with sources such as crude oil, urban dust, sedimentary rocks, and cigarette smoke (Kracher et al., 1988). BeP originates from the combustion of coal, wood, oil, and cigarette smoke (Dean et al., 2022). Notably, BeP is more resistant to photochemical degradation than its isomer BaP (Lee et al., 2001). Thus, the BeP/BaP ratio is often used as an indicator of atmospheric aging of PAHs (Lee et al., 2006). BeP was rarely detected in Yeongil Bay, making the BeP/BaP ratio unmeasurable in this region. In contrast, at all sites in the Hupo Basin, except for H25, the BeP/BaP ratio exceeded 1.0, indicating the presence of photochemically aged PAHs deposited following long-range atmospheric transport (Fig. S4) (Lee et al., 2006). The H25 site, located at the northernmost end, showed a

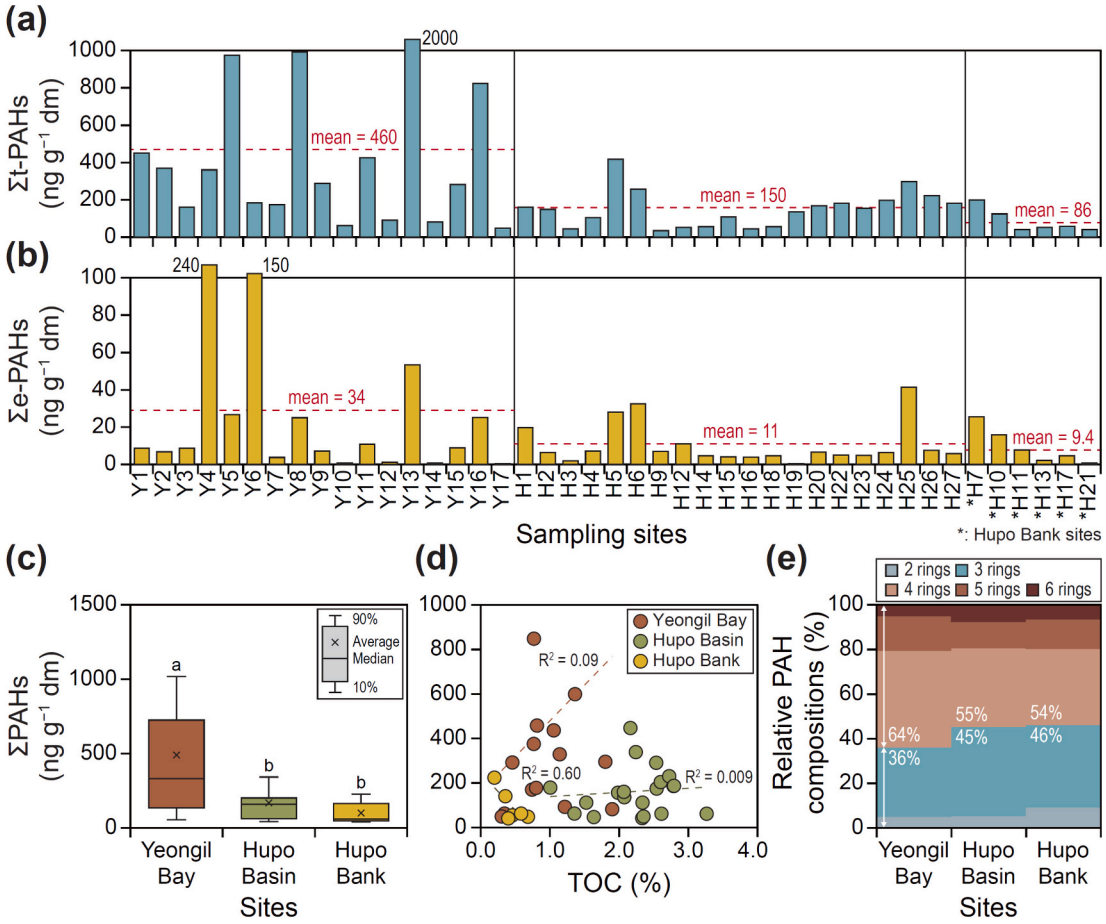

Fig. 2. (a) Concentrations of t-PAHs and (b) e-PAHs in surface sediments from the Yeongil Bay, the Hupo Basin, and the Hupo Bank, East Sea. (c) Box plots of total PAH concentrations by region. Different letters indicate statistically significant differences among regions ($p < 0.05$, Kruskal-Wallis test). (d) Correlation between TOC and PAH concentrations in surface sediments. (e) Relative compositions of PAHs by regions of the study area.

lower ratio of ~0.74, suggesting recent or more locally derived PAH input.

In Yeongil Bay, PAH concentrations exhibited a positive correlation with TOC, whereas the Hupo Basin showed little correlation, and the Hupo Bank displayed a negative correlation (Fig. 2d). Although PAHs in sediments are generally positively correlated with TOC content (Rockne et al., 2002), this trend was not evident in the Hupo Bank. Given the limited number of samples from the Hupo Bank, this result should be interpreted with caution; nonetheless, it may reflect the unique geomorphological setting and hydrodynamic conditions, which hinder organic matter deposition and PAH preservation (Kim and Park, 2014). Analysis of PAH composition showed that high molecular weight (HMW) PAHs (4–6 rings) accounted for approximately 64% of total PAHs in Yeongil Bay, decreasing to 55% in the Hupo Basin and 54% in the Hupo Bank (Fig. 2e). This trend likely reflects the greater solubility and volatility of low molecular weight (LMW) PAHs, which facilitate long-range atmospheric and oceanic transport (Wania and Mackay, 1996). Overall, the spatial distribution and composition of PAHs across the study area appear to be influenced by geomorphological characteristics, depositional conditions, and the physicochemical properties of PAHs.

3.3. Potential sources of PAHs in surface sediments

PLS analysis was conducted to identify spatial distribution patterns and major contributing factors based on TOC, TN, and individual PAHs concentrations in sediments (Fig. S5). The results showed a clear division of the study area into three distinct clusters, Yeongil Bay, the Hupo Basin, and the Hupo Bank, reflecting not only geographic separation but also differences in organic matter composition and PAH profiles. Parameters with variable importance in projection (VIP) scores above 1.0 were considered statistically significant in differentiating the regions (Farrés et al., 2015). TN and TOC exhibited the highest VIP scores, indicating that they were key factors driving sediment differentiation across the study area (Fig. S5). Among the PAHs, 3-ring PAHs such as 9-ethylphenanthrene and Phe also had relatively high VIP scores, suggesting that these LMW PAHs contributed to regional variability. PCA supported the PLS findings, showing a distinct separation of the three regions based on compositional differences (Fig. S5). Along PC1 (52%) and PC2 (27%), Yeongil Bay (Group 1) was positively associated with 2-ring and 5-ring PAHs, while sediments from the Hupo Basin were closely linked to TOC and TN. Meanwhile, 3-ring, 4-ring, and 6-ring PAHs showed moderate associations with both regions. The Hupo Bank (Group 3) exhibited weak negative correlations with most variables, suggesting a distinct and isolated environmental profile.

To further explore the relationships between biogeochemical indicators and PAHs, Spearman's rank correlation analysis was conducted for compounds detected in more than 70% of sediment samples (Fig. S6). In Yeongil Bay sediments, most PAHs exhibited positive correlations with biogeochemical parameters, consistent with the general trend of PAH accumulation in organic-rich environments. However, significant negative correlations were observed between $\delta^{13}C$ values and several individual PAHs, suggesting contributions from terrestrial organic matter (Hong et al., 2022b). In contrast, sediments from the Hupo Basin showed a different pattern: most biogeochemical indicators, including TOC, TN, $\delta^{13}C$, and $\delta^{15}N$, were negatively correlated with PAHs. A similar trend was observed in the Hupo Bank sediments. These results may reflect differing conditions of organic matter accumulation and/or external PAH sources in the Hupo region. Although not statistically significant, some LMW PAHs showed negative correlations among themselves, while HMW PAHs tended to exhibit positive intercorrelations.

To identify the potential sources of PAHs in surface sediments, PMF modeling was conducted separately for Yeongil Bay and the Hupo region, as the PAH distribution patterns differed significantly between the two areas. In Yeongil Bay, three factors were extracted and identified as vehicle emissions (Factor 1), indicated by high loading of dibenz[*a,h*] anthracene (DbahA); coal combustion (Factor 2), characterized by chrysene (Chr); and steel production (Factor 3), reflected by elevated BaP levels (Ravindra et al., 2008) (Fig. 3a). Similarly, three major factors were identified in the Hupo region: vehicle emissions (Factor 1), with notable DbahA contributions; biomass combustion (Factor 2), marked by anthracene; and coal combustion (Factor 3), represented by Chr (Harrison et al., 1996; Ravindra et al., 2008) (Fig. 3b). In both regions, vehicle emissions and coal combustion were the dominant sources. However, steel production was uniquely identified in Yeongil Bay, likely reflecting the influence of large-scale steel manufacturing facilities located in the region (Shin and Ciccantell, 2009). In particular, the high contribution of BaP is consistent with emissions from high-temperature combustion processes in the steel industry (Khaparde et al., 2016). In the Hupo region, biomass combustion was identified as a significant source, possibly associated with the frequent seasonal forest fires that occur in spring (Choung et al., 2004).

The spatial distribution of source contributions in Yeongil Bay showed distinct regional patterns (Fig. 3c). For instance, Y1–Y6, except for Y3, were predominantly influenced by vehicle emissions, likely due to their proximity to urban areas and major roadways. In contrast, Y7–Y12 were affected by emissions from steel manufacturing processes, reflecting the impacts from nearby industrial complexes. Meanwhile, coal combustion contributed relatively evenly across all sites without dominating any single location, indicating its role as a diffuse background source likely linked to residential heating, energy production, and industrial fuel use (Park et al., 2021). The relative source contributions also differed between the Hupo Basin and the Hupo Bank (Fig. 3d). Coal combustion accounted for the highest proportion in the Hupo Basin (36%), and vehicle emissions were dominant in the Hupo Bank, averaging 50%. Interestingly, source contributions within the Hupo region varied depending on proximity to Yeongil Bay. Sites H1–H6, located closer to Yeongil Bay, showed a stronger vehicle influence. In contrast, the northern sites exhibited a higher proportion of coal combustion, with biomass combustion being dominant at a few locations. The Hupo region extends longitudinally along the coast, with some sites near Yeongil Bay and others closer to population centers such as Yeongdeok and Uljin. These geographic and anthropogenic factors likely explain the observed variation in source contributions across the Hupo region.

3.4. Potential ecological risks of PAHs in surface sediments

The potential ecological risks of PAHs in sediments were evaluated using the HQ approach, and the total HQ_{sum} was calculated for each site (Fig. 4a). All sites exhibited HQ_{sum} values below 1.0, indicating low immediate ecological risk under current conditions. However, when applying a more conservative threshold of $HQ_{sum} > 0.1$, often used to indicate low to moderate risk, several sites showed potential concern. In Yeongil Bay, sites Y5, Y8, Y13, and Y16 exceeded this threshold, with Y13 showing the highest HQ_{sum} value of 0.45, suggesting notable PAHs accumulation and localized ecological stress. In contrast, most sites in the Hupo region had HQ_{sum} values below 0.1, except for H25. At these sites (Y5, Y8, Y13, Y16, and H25), HMW PAHs, such as benzo[*g,h,i*] perylene (BghiP) and indeno[*1,2,3-cd*]pyrene (IcdP), were identified as the major contributors to the calculated HQ_{sum} (Fig. 4b). Notably, t-PAHs accounted for approximately 99% of the HQ_{sum} at Yeongil Bay sites, whereas e-PAHs contributed about 10% to the HQ_{sum} at H25. Among the e-PAHs, BeP (8.4%) showed a relatively high contribution, likely due to its resistance to photochemical degradation and prolonged atmospheric residence time (Lee et al., 2001). Although this study used model-derived toxicity values to assess potential ecological risks, which represents a limitation, the results highlight that e-PAHs, which are often excluded from traditional risk assessment, may contribute meaningfully to overall ecological risk.

In addition, the BaP-TEQ and BaP-MEQ values were calculated for

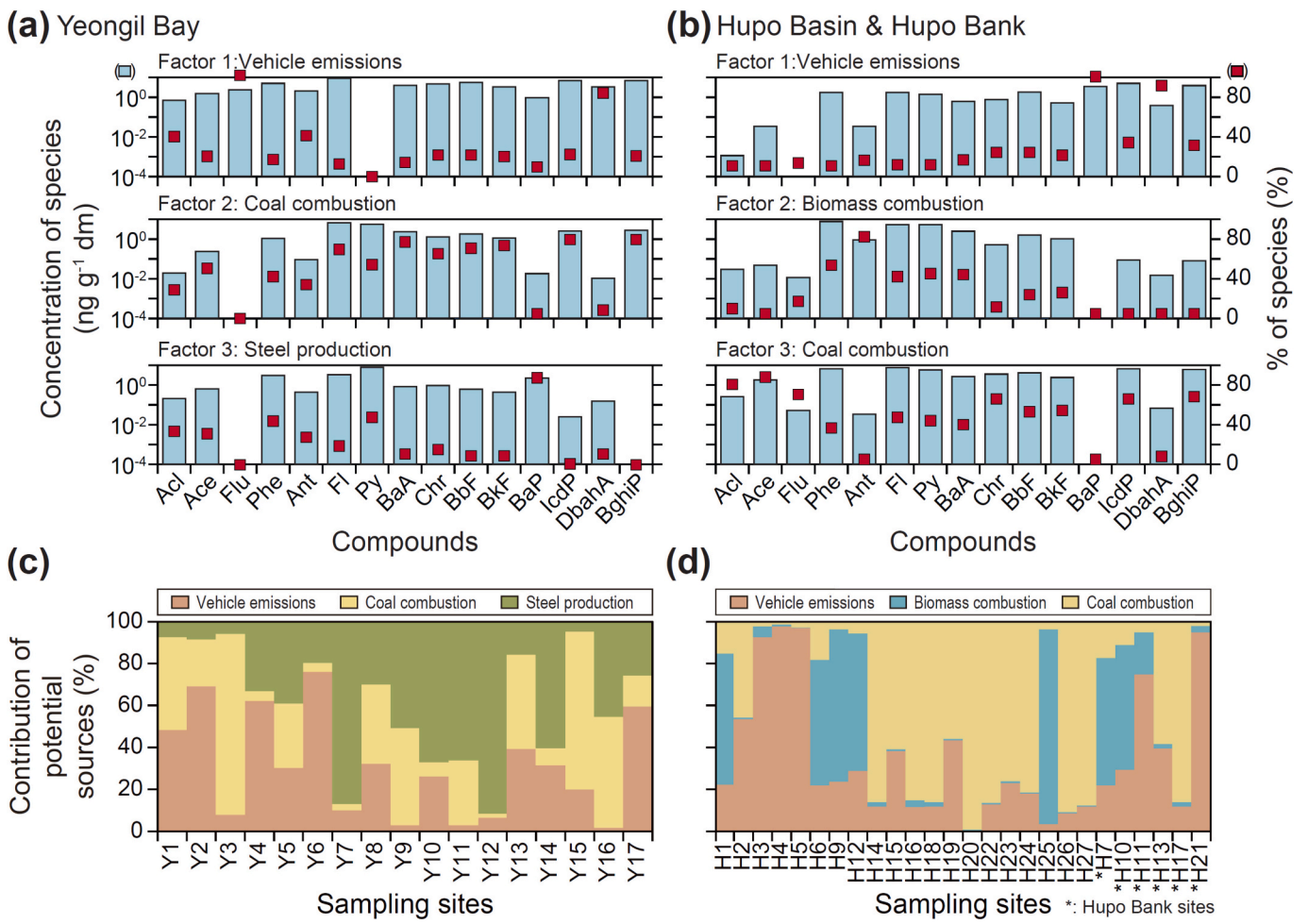

Fig. 3. Estimated source profiles and contributions of PAHs in sediments using the positive matrix factorization (PMF) modeling. (a) Three major sources identified in Yeongil Bay: vehicle emissions (Factor 1), coal combustion (Factor 2), and steel production activities (Factor 3). (b) Major PAHs sources in the Hupo Basin and the Hupo Bank: vehicle emissions (Factor 1), biomass combustion (Factor 2), and coal combustion (Factor 3). (c) Relative contributions of each source to PAH concentrations at individual sites in Yeongil Bay and (d) the Hupo Basin and the Hupo Bank.

the eight target PAHs to evaluate their potential carcinogenic and mutagenic toxicities (Tables S8 and S9). The mean BaP-TEQ values in Yeongil Bay, the Hupo Basin, and the Hupo Bank were 36, 9.1, and 7.2 ng g^{-1} dm, respectively, with particularly high values observed at Y13 (120 ng g^{-1} dm) and Y8 (110 ng g^{-1} dm). BaP (53%) and dibenzo[*a,h*] anthracene (DbahA, 26%) were the dominant contributors to the total BaP-TEQ values. The predominance of BaP and DbahA in contributing to BaP-TEQ values in sediments is consistent with previous findings (Zafeiraki et al., 2023). The BaP-MEQ values in Yeongil Bay (46 ng g^{-1} dm) were approximately 3–5 times higher than those in the Hupo Basin (15 ng g^{-1} dm) and the Hupo Bank (10 ng g^{-1} dm). Similarly, the highest BaP-MEQ value was found at Y13 (180 ng g^{-1} dm) in Yeongil Bay. Within the Hupo region, H25 (80 ng g^{-1} dm) also exhibited a relatively high value. Among the target PAHs, BaP and IcdP accounted for approximately 46% and 19% of the total BaP-MEQ values, respectively, which is in line with previous observations (Ihunwo et al., 2021). These results from the potential ecological risks assessment indicate that HMW PAHs, such as BghiP, IcdP, and BaP, are the major contributors, highlighting the need for management strategies to mitigate their impacts.

3.5. *Historical trends of PAHs recorded in core sediments*

Temporal trends of PAHs were investigated in core sediments from four sites (H8, H15, H20, and H25) in the Hupo Basin, categorized into three time periods: 1940 to 1975, 1975 to 1995, and 1995 to the present (Fig. S7 and Table S10) (Joe et al., 2022). The average TOC content was highest at H20 (2.2%) and H25 (2.2%), followed by H8 (1.7%) and H15 (1.2%), and remained relatively stable over time, without a distinct increasing or decreasing trend. PAH concentrations were highest at H8 (230 ng g^{-1} dm), showing a temporary decrease during 1975–1995, followed by a subsequent increase. Despite its relatively low TOC content, H8 exhibited high PAH concentrations, likely due to its proximity to Yeongil Bay and a low sedimentation rate, which may have promoted PAHs accumulation and preservation. In general, areas with low sedimentation rates provide favorable conditions for the deposition and long-term retention of hydrophobic pollutants such as PAHs (Lloyd et al., 2024). At H15, PAH concentrations steadily increased after 1975, along with a slight increase in the proportion of HMW PAHs. This trend may reflect increased industrial emissions or enhanced atmospheric deposition during that period (Khaparde et al., 2016). H20, which had the highest TOC content, also showed relatively high average PAH concentrations (214 ng g^{-1} dm), with minimal variation across the three periods. The compositional profiles of PAHs at this site remained largely consistent over time. At H25, PAH concentrations increased markedly after 1995, along with a gradual rise in the proportion of HMW PAHs. This increase may partly reflect the influence of PAHs released during the construction of a nearby nuclear power plant in the 1980s (Kim et al., 2008), likely associated with the use of heavy machinery and fuel combustion.

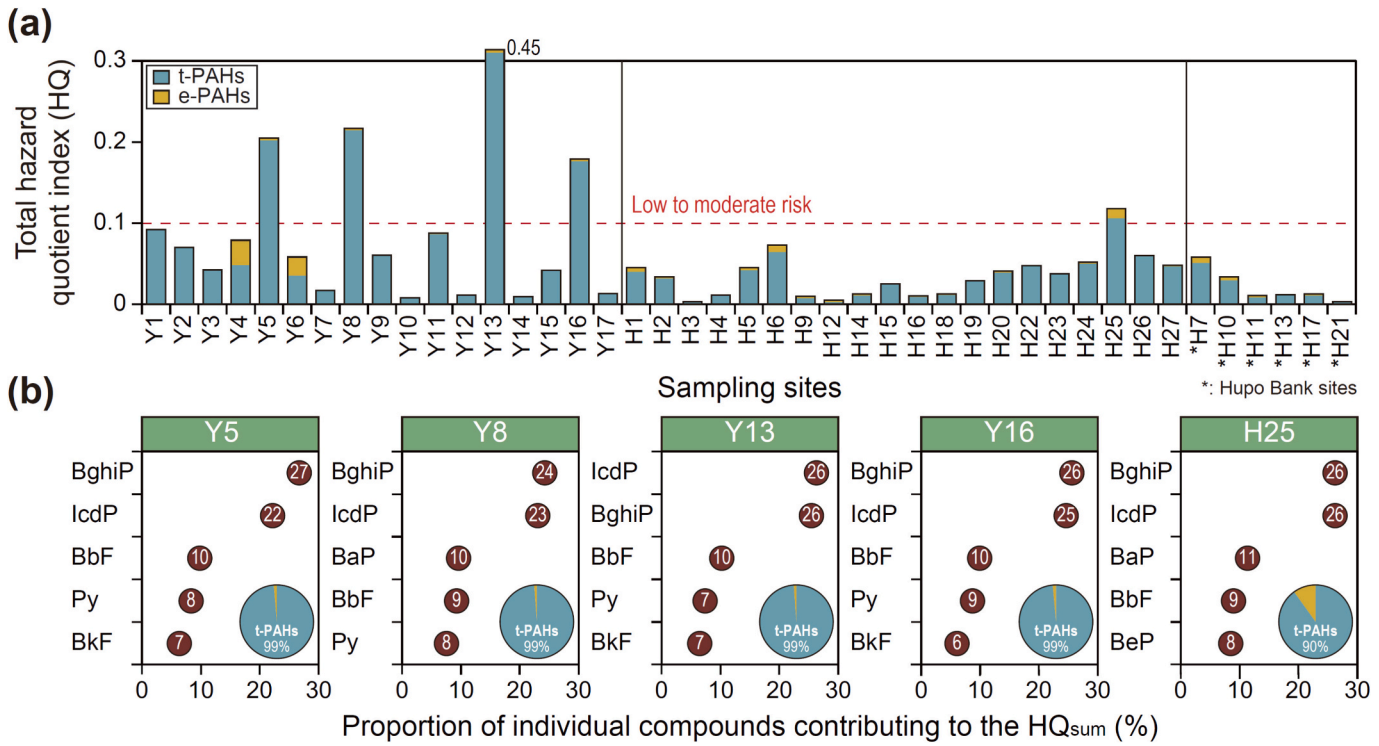

Fig. 4. (a) Hazard quotient (HQ) values for total PAHs at each sampling site of surface sediments from Yeongil Bay, the Hupo Basin, and the Hupo Bank, East Sea. The red dashed line (HQ = 0.1) represents the threshold for potential ecological concern. (b) Relative contributions of individual PAHs to total HQ (HQ_{sum}) at selected sites (Y5, Y8, Y13, Y16, and H25) where HQ > 0.1. (For interpretation of the references to colour in this figure legend, the reader is referred to the web version of this article.)

3.6. Source apportionment and anthropogenic fluxes of PAHs

Based on the three PAH source profiles (vehicle emissions, biomass combustion, and coal combustion) identified through PMF analysis of surface sediments, historical source contributions and anthropogenic PAH fluxes were assessed (Fig. 5 and Fig. S8). In core H8, coal combustion was the dominant contributor during the 1940s, consistent with the historical reliance on coal for residential heating and fuel use (Kimura, 2018). Since the 1960s, the contribution from vehicle-related emissions has gradually increased, becoming the primary source in later decades. This trend reflects rapid urbanization, industrialization, and the expansion of transportation infrastructure in South Korea (Eom and Schipper, 2010; Yoo, 2017). It is also aligned with national developments, as South Korea experienced extensive road construction and a sharp increase in vehicle use after the 1960s (Song et al., 2023). Notably, the annual cargo throughput at major East Sea ports rose from several hundred thousand tons in the late 1960s to over ten million tons by the 1980s (Song et al., 2023). Despite these shifts in source contributions, the anthropogenic PAH flux at H8 remained relatively stable over time. Similar trends were observed at H15, where coal combustion was dominant before 1975, followed by a marked increase in vehicle emission contributions. The PAH flux at this site increased nearly fourfold, from 12 ng m^{-2} y^{-1} to 51 ng m^{-2} y^{-1} after 1975, suggesting either enhanced sedimentary accumulation or intensified emission inputs.

In contrast, cores H20 and H25 consistently exhibited relatively high contributions from biomass combustion throughout the study period. This pattern may reflect the influence of frequent large-scale wildfires and extensive forested areas along the eastern coast of Korea (Choung et al., 2004). For instance, in 2000, a massive wildfire burned approximately 23,794 ha of forest across regions such as Goseong, Gangneung,

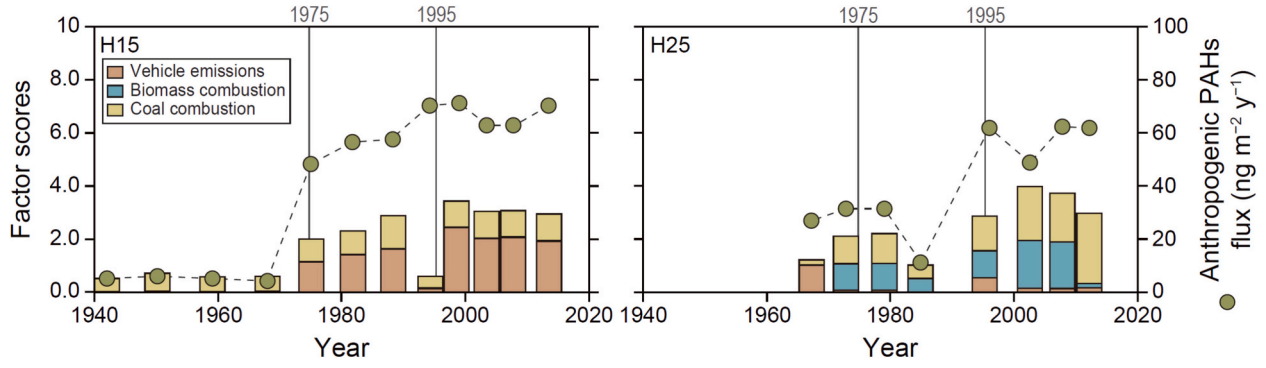

Fig. 5. Temporal variations in the relative contributions of PAH sources in core sediments from two sites (H15 and H25) in the Hupo Basin, as estimated by PMF modeling. Stacked bars represent the proportions of vehicle emissions, biomass combustion, and coal combustion. Green circles indicate anthropogenic PAH fluxes (ng m^{-2} y^{-1}) at each sediment depth. Results for cores H8 and H20 are shown in Fig. S8 of the Supplementary Materials. (For interpretation of the references to colour in this figure legend, the reader is referred to the web version of this article.)

Donghae, Samcheok, and Uljin, potentially leaving long-term impacts on PAHs deposition in marine sediments (Choung et al., 2004). At H20, both source contributions and anthropogenic PAH fluxes remained stable across all three time periods. In contrast, core H25 exhibited a different pattern, with vehicle emissions dominating in the 1960s, followed by a gradual increase in coal combustion contributions. This divergence from the trends observed at H8 and H15 may reflect localized environmental conditions and differences in emission sources. Furthermore, the anthropogenic flux at H25 increased nearly fourfold after 1980, indicating a substantial intensification of PAHs input in recent decades. This may suggest that PAHs input associated with power plant construction during this period should be considered. Globally, PAH emissions have steadily declined since the mid-1990s (Shen et al., 2013). However, the recent trends observed in this study differ from global patterns, suggesting that the region continues to be influenced by both intentional and unintentional PAH emissions. For example, a newly constructed passenger terminal near the Hupo region may be a potential contributor, although its impact on PAH levels requires further investigation.

3.7. Comparison with previous studies

In this study, PAH concentrations in surface sediments were compared with those reported in previous studies conducted across various aquatic environments in Korea, including creeks, rivers, lakes, bays, and coastal zones (Table 1). To ensure valid comparisons, reference studies conducted within a similar timeframe (approximately ±10 years) were selected. The results showed that PAH concentrations in Yeongil Bay were relatively elevated compared to most other regions in Korea. Although some inland creek sites exhibited higher concentrations, this is likely due to the localized and concentrated nature of pollution sources in such environments (Cha et al., 2019). Notably, when compared with other bay areas such as Jinhae Bay, Ulsan Bay, and Gyeonggi Bay, PAH concentrations in Yeongil Bay were approximately 4–10 times higher. Furthermore, in comparison with a previous study that analyzed PAHs in Yeongil Bay sediments collected in 2018, the concentrations reported in this study were higher, despite a smaller number of target compounds. This discrepancy may be attributed to differences in sampling locations and spatial heterogeneity in pollution sources. In addition, the present study offers enhanced spatial resolution by including a greater number of sampling sites across Yeongil Bay, enabling a more comprehensive assessment of pollution distribution.

In the Hupo region, PAH concentrations were generally lower than those reported in riverine and bay sediments from other regions of South Korea. However, when compared with other coastal or marine environments, such as the Taean coast, Yellow Sea, and South Sea, the Hupo region showed relatively higher concentrations. This finding is consistent with previous reports indicating that sediment PAH levels in the East Sea are generally higher than those in the West and South Seas of Korea, possibly due to the higher TOC content in East Sea sediments, which promotes PAHs accumulation (Kim et al., 2021). Overall, this comparison highlights the relative pollution status of PAHs in the study area and provides important context for developing region-specific sediment management strategies.

4. Conclusions

This study examined the spatiotemporal distribution, source apportionment, and ecological risks of PAHs in sediments from the East Sea of Korea. The contrasting levels of industrialization and hydrodynamic conditions between Yeongil Bay and the Hupo region provided insights into how local factors influence PAH contamination along the coast. Region-specific PAH distribution patterns were shaped by sediment characteristics, proximity to pollution sources, and localized hotspots, reflecting the complexity of coastal contamination mechanisms. PAHs have been present in sediments since the pre-industrial era and continue to accumulate despite recent environmental mitigation efforts. This highlights the need for sustained monitoring and effective sediment management. Clarifying whether PAH inputs are primarily from local emissions or long-range transport remains essential. Further studies using isotopic analysis or source-specific tracers are recommended to refine source apportionment and support targeted management strategies. Overall, this study provides a comprehensive understanding of PAH contamination in coastal sediments, offering a valuable scientific basis

Table 1
Concentrations of PAHs in surface sediments from the bay and coastal regions of Korea obtained from this study and previous studies.

Region	Type	Sampling year	# of sites	# of targets	Concentrations (ng g^{-1} dm)			References
					Min	Max	Mean	
Jinhae Bay	Bay	2010	80	22	12	2400	110	Hong et al. (2014a)
Lake Ansan	Lake	2010–2014	2	15	1.5	42	14	Jeon et al. (2017)
Lake Sapgyo	Lake		2		4.7	81	25	
Taean	Coastal		3		1.3	7.7	3.0	
Geum River	River		2		20	93	53	
Yeongsan River	Lake	2011	1	16	–	–	270	Lee et al. (2022)
	Creek		6		88	1400	550	
	Estuary		9		84	270	200	
Nakdong River	Lake		1		–	–	250	
	Creek		6		42	1400	670	
	Estuary		7		53	320	160	
Busan Coast	River and Harbor	2013	37	16	3.9	5300	390	Han et al. (2016)
Saemangeum Coast	Estuary and bay	2014	58	24	2.9	160	39	Yoon et al. (2017)
Masan Bay	Bay	2014	9	16	25	1900	91	Lee et al. (2018)
Lake Sihwa	Creek	2014, 2017	8	15	14	1400	340	Cha et al. (2019)
Ulsan Bay	River and creek	2017	4	15	31	1270	510	An et al. (2020)
	Bay		5		35	78	53	
Yellow Sea	Sea	2017	18	24	14	150	44	Kim et al. (2021)
South Sea	Sea	2018	10		31	150	75	
East Sea	Sea	2017	6		40	700	340	
Yeongil Bay	River	2018	1	29	–	–	290	Gwak et al. (2022)
	Bay		4		3.3	110	43	
Gyeonggi Bay	Bay	2018	58	30	22	354	78	Song et al. (2025)
Incheon Port	Bay		15		66	520	170	
Yeongil Bay	Bay	2014	17	23	50	2100	490	This study
Hupo Basin	Coastal	2017	20		43	400	160	
Hupo Bank	Coastal		6		42	220	96	

for pollution control, policy development, and long-term environmental monitoring.

CRediT authorship contribution statement

Jihyun Cha: Writing – original draft, Visualization, Investigation, Formal analysis, Data curation, Conceptualization. **Chang-Eon Lee:** Writing – original draft, Visualization, Investigation, Formal analysis, Conceptualization. **Mungi Kim:** Investigation, Formal analysis. **Youngnam Kim:** Investigation, Formal analysis. **Jiyun Gwak:** Investigation, Formal analysis. **Dong Jin Joe:** Investigation, Data curation. **Jae-Hyun Lim:** Funding acquisition, Formal analysis. **In Kwon Um:** Investigation, Funding acquisition, Formal analysis. **Man Sik Choi:** Methodology, Funding acquisition, Formal analysis, Data curation. **Seongjin Hong:** Writing – review & editing, Supervision, Methodology, Investigation, Funding acquisition, Formal analysis, Conceptualization.

Declaration of competing interest

The authors declare that they have no known competing financial interests or personal relationships that could have appeared to influence the work reported in this paper.

Acknowledgments

This study was supported by grants from the National Research Foundation of Korea (RS-2024-00322608) and the Ministry of Oceans and Fisheries of Korea (RS-2023-00256330). Additional support was provided by the National Institute of Fisheries Science (R2025015).

Appendix A. Supplementary data

Supplementary data to this article can be found online at https://doi.org/10.1016/j.marpolbul.2025.118713.

Data availability

Data will be made available on request.

References

An, Y., Hong, S., Yoon, S.J., Cha, J., Shin, K.-H., Khim, J.S., 2020. Current contamination status of traditional and emerging persistent toxic substances in the sediments of Ulsan Bay, South Korea. Mar. Pollut. Bull. 160, 111560. https://doi.org/10.1016/j.marpolbul.2020.111560.

An, S.-A., Hong, S., Lee, J., Cha, J., Lee, S., Moon, H.-B., Giesy, J.P., Khim, J.S., 2021. Identification of potential toxicants in sediments from an industrialized area in Pohang, South Korea: application of a cell viability assay of microalgae using flow cytometry. J. Hazard. Mater. 405, 124230. https://doi.org/10.1016/j.jhazmat.2020.124230.

Balmer, J.E., Hung, H., Yu, Y., Letcher, R.J., Muir, D.C.G., 2019. Sources and environmental fate of pyrogenic polycyclic aromatic hydrocarbons (PAHs) in the Arctic. Emerg. Contam. 5, 128–142. https://doi.org/10.1016/j.emcon.2019.04.002.

Cha, J., Hong, S., Kim, J., Lee, J., Yoon, S.J., Lee, S., Moon, H.-B., Shin, K.-H., Hur, J., Giesy, J.P., Khim, J.S., 2019. Major AhR-active chemicals in sediments of Lake Sihwa, South Korea: application of effect-directed analysis combined with full-scan screening analysis. Environ. Int. 133, 105199. https://doi.org/10.1016/j.envint.2019.105199.

Cha, J., Kim, J.-H., Jung, J.Y., Nam, S.-I., Hong, S., 2024. Chronological distribution and potential sources of persistent toxic substances in soils from the glacier foreland of Midtre Lovénbreen, Svalbard. Environ. Pollut. 357, 124387. https://doi.org/10.1016/j.envpol.2024.124387.

Choung, Y., Lee, B.-C., Cho, J.-H., Lee, K.-S., Jang, I.-S., Kim, S.-H., Hong, S.-K., Jung, H.-C., Choung, H.-L., 2004. Forest responses to the large-scale east coast fires in Korea. Ecol. Res. 19, 43–54. https://doi.org/10.1111/j.1440-1703.2003.00607.x.

Dean, J.L., Angrish, M., Mezencev, R., 2022. Provisional peer-reviewed toxicity values for Benzo[e]pyrene (BeP)(CASRN 192-97-2).

Durant, J.L., Busby Jr., W.F., Lafleur, A.L., Penman, B.W., Crespi, C.L., 1996. Human cell mutagenicity of oxygenated, nitrated and unsubstituted polycyclic aromatic hydrocarbons associated with urban aerosols. Mutat. Res. Genet. Toxicol. 371, 123–157. https://doi.org/10.1016/S0165-1218(96)90103-2.

Durant, J.L., Lafleur, A.L., William, F.B.J., Lawrence, L.D., Bruce, W.P., Charles, L.C., 1999. Mutagenicity of C24H14 PAH in human cells expressing CYP1A1. Mutat. Res. 446, 1–14. https://doi.org/10.1016/S1383-5718(99)00135-7.

Eom, J., Schipper, L., 2010. Trends in passenger transport energy use in South Korea. Energ Policy 38, 3598–3607. https://doi.org/10.1016/j.enpol.2010.02.037.

Farrés, M., Platikanov, S., Tsakovski, S., Tauler, R., 2015. Comparison of the variable importance in projection (VIP) and of the selectivity ratio (SR) methods for variable selection and interpretation. J. Chemom. 29, 528–536. https://doi.org/10.1002/cem.2736.

Gao, X., Li, J., Wang, X., Zhou, J., Fan, B., Li, W., Liu, Z., 2019. Exposure and ecological risk of phthalate esters in the Taihu Lake basin, China. Ecotox. Environ. Safe. 171, 564–570. https://doi.org/10.1016/j.ecoenv.2019.01.001.

Gwak, J., Cha, J., Lee, J., Kim, Y., An, S.-A., Lee, S., Moon, H.-B., Hur, J., Giesy, J.P., Hong, S., Khim, J.S., 2022. Effect-directed identification of novel aryl hydrocarbon receptor-active aromatic compounds in coastal sediments collected from a highly industrialized area. Sci. Total Environ. 803, 149969. https://doi.org/10.1016/j.scitotenv.2021.149969.

Gwak, J., Cha, J., Nam, S.-I., Kim, J.-H., Lee, J., Moon, H.-B., Khim, J.S., Hong, S., 2024. Characterization of AhR-mediated potency in sediments from Kongsfjorden, Svalbard: application of effect-directed analysis and nontarget screening. Chemosphere 368, 143771. https://doi.org/10.1016/j.chemosphere.2024.143771.

Han, G.M., Hong, S.H., Shim, W.J., Ra, K.T., Kim, K.T., Ha, S.Y., Jang, M., Kim, G.B., 2016. Assessment of persistent organic and heavy metal contamination in Busan coast: application of sediment quality index. Ocean Polar Res. 38, 171–184. https://doi.org/10.4217/OPR.2016.38.3.171.

Harrison, R.M., Smith, D.J.T., Luhana, L., 1996. Source apportionment of atmospheric polycyclic aromatic hydrocarbons collected from an urban location in Birmingham, U.K. Environ. Sci. Technol. 30, 825–832. https://doi.org/10.1021/es950252d.

Hong, S.H., Han, G.M., Yim, U.H., Lim, D.-i., Ha, S.Y., Kim, N.S., Shim, W.J., 2014a. Integrative assessment of sediment quality in terms of chemical contamination in Jinhae Bay, South Korea. Ocean Sci. J. 49, 265–278. https://doi.org/10.1007/s12601-014-0027-4.

Hong, S., Khim, J.S., Park, J., Kim, S., Lee, S., Choi, K., Kim, C.S., Choi, S.D., Park, J., Ryu, J., Jones, P.D., Giesy, J.P., 2014b. Instrumental and bioanalytical measures of dioxin-like compounds and activities in sediments of the Pohang Area, Korea. Sci. Total Environ. 470–471, 1517–1525. https://doi.org/10.1016/j.scitotenv.2013.06.112.

Hong, S.-H., Yoo, D.-G., Lee, G.-S., Kim, J.C., Yi, S., Kim, G.-Y., Bahk, J.-J., Yu, S., 2022a. Late pliocene to quaternary sedimentary facies and stratigraphy of shallow-water contourite deposits in the Hupo Basin, East Sea of Korea. Mar. Geophys. Res. 43, 38. https://doi.org/10.1007/s11001-022-09499-5.

Hong, S., Kim, Y., Lee, Y., Yoon, S.J., Lee, C., Liu, P., Kwon, B.-O., Hu, W., Khim, J.S., 2022b. Distributions and potential sources of traditional and emerging polycyclic aromatic hydrocarbons in sediments from the lower reach of the Yangtze River, China. Sci. Total Environ. 815, 152831. https://doi.org/10.1016/j.scitotenv.2021.152831.

Ihunwo, O.C., Ibezim-Ezeani, M.U., DelValls, T.A., 2021. Human health and ecological risk of polycyclic aromatic hydrocarbons (PAHs) in sediment of Woji creek in the Niger Delta region of Nigeria. Mar. Pollut. Bull. 162, 111903. https://doi.org/10.1016/j.marpolbul.2020.111903.

Jeon, S., Hong, S., Kwon, B.-O., Park, J., Song, S.J., Giesy, J.P., Khim, J.S., 2017. Assessment of potential biological activities and distributions of endocrine-disrupting chemicals in sediments of the west coast of South Korea. Chemosphere 168, 441–449. https://doi.org/10.1016/j.chemosphere.2016.10.089.

Joe, D.J., Choi, M.S., Um, I.K., Choi, S.H., Park, S.J., 2022. Mercury contamination of sediments in an open coastal area of the Hupo Basin, East Sea, Korea. Mar. Pollut. Bull. 182, 113980. https://doi.org/10.1016/j.marpolbul.2022.113980.

Khaparde, V.V., Bhanarkar, A.D., Majumdar, D., Rao, C.V.C., 2016. Characterization of polycyclic aromatic hydrocarbons in fugitive PM10 emissions from an integrated iron and steel plant. Sci. Total Environ. 562, 155–163. https://doi.org/10.1016/j.scitotenv.2016.03.153.

Kim, C.H., Park, C.H., 2014. Detailed bathymetry and seabed characteristics of Wangdol-cho, Hupo Bank in the East sea. Econ. Environ. Geol. 47, 533–540. https://doi.org/10.9719/EEG.2014.47.5.533.

Kim, Y.S., Choi, H.G., Nam, K.W., 2008. Seasonal variations of marine algal community in the vicinity of Uljin nuclear power plant, Korea. J. Environ. Biol. 94, 493–499.

Kim, J., Hong, S., Cha, J., Lee, J., Kim, T., Lee, S., Moon, H.-B., Shin, K.-H., Hur, J., Lee, J.-S., Giesy, J.P., Khim, J.S., 2019. Newly identified AhR-active compounds in the sediments of an industrial area using effect-directed analysis. Environ. Sci. Technol. 53, 10043–10052. https://doi.org/10.1021/acs.est.9b02166.

Kim, Y., Hong, S., Lee, J., Yoon, S.J., An, Y., Kim, M.-S., Jeong, H.-D., Khim, J.S., 2021. Spatial distribution and source identification of traditional and emerging persistent toxic substances in the offshore sediment of South Korea. Sci. Total Environ. 789, 147996. https://doi.org/10.1016/j.scitotenv.2021.147996.

Kim, Y., Cha, J., Shin, G., Wang, T., Hu, W., Khim, J.S., Hong, S., 2025. Spatial distribution and potential ecological risk of traditional and emerging organic toxic substances in sediments along the Yangtze River, China. Mar. Pollut. Bull. 219, 118283. https://doi.org/10.1016/j.marpolbul.2025.118283.

Kimura, M., 2018. Colonial development of modern industry in Korea, 1910-1939/40. Jpn. Rev. 2, 23–44.

Kracher, W., Ellison, S., Ewald, M., Garrigues, P., Gevers, E., Jacob, J., 1988. Spectral Atlas of Polycyclic Aromatic Compounds: Including Data on Physico-Chemical Properties, Occurrence and Biological Activity. Kluwer Academic Publishers.

Lee, S.C., Ho, K.F., Chan, L.Y., Zielinska, B., Chow, J.C., 2001. Polycyclic aromatic hydrocarbons (PAHs) and carbonyl compounds in urban atmosphere of Hong Kong. Atmos. Environ. 35, 5949–5960. https://doi.org/10.1016/S1352-2310(01)00374-0.

Lee, J.Y., Kim, Y.P., Kang, C.-H., Ghim, Y.S., Kaneyasu, N., 2006. Temporal trend and long-range transport of particulate polycyclic aromatic hydrocarbons at Gosan in Northeast Asia between 2001 and 2004. J. Geophys. Res. Atmos. 111. https://doi.org/10.1029/2005JD006537.

Lee, J., Hong, S., Kwon, B.-O., Cha, S.A., Jeong, H.-D., Chang, W.K., Ryu, J., Giesy, J.P., Khim, J.S., 2018. Integrated assessment of persistent toxic substances in sediments from Masan Bay, South Korea: comparison between 1998 and 2014. Environ. Pollut. 238, 317–325. https://doi.org/10.1016/j.envpol.2018.02.064.

Lee, J., Cha, J., Yoon, S.J., Hong, S., Khim, J.S., 2022. Instrumental and bioanalytical characterization of dioxin-like activity in sediments from the Yeongsan River and the Nakdong River estuaries, South Korea. Sci. Total Environ. 826, 154240. https://doi.org/10.1016/j.scitotenv.2022.154240.

Lemly, A.D., 1996. Evaluation of the hazard quotient method for risk assessment of selenium. Ecotox. Environ. Safe. 35, 156–162. https://doi.org/10.1006/eesa.1996.0095.

Li, B., Liu, R., Gao, H., Tan, R., Zeng, P., Song, Y., 2016. Spatial distribution and ecological risk assessment of phthalic acid esters and phenols in surface sediment from urban rivers in Northeast China. Environ. Pollut. 219, 409–415. https://doi.org/10.1016/j.envpol.2016.05.022.

Li, Y., Guo, N., Yuan, K., Chen, B., Wang, J., Hua, M., Yu, J., Hu, J., Lu, R., Zou, S., Yang, Y., 2023. Variations in the concentration, source and flux of polycyclic aromatic hydrocarbons in sediments of the Pearl River estuary: implications for anthropogenic impacts. Sci. Total Environ. 862, 160870. https://doi.org/10.1016/j.scitotenv.2022.160870.

Liu, L.-Y., Wang, J.-Z., Wei, G.-L., Guan, Y.-F., Wong, C.S., Zeng, E.Y., 2012. Sediment records of polycyclic aromatic hydrocarbons (PAHs) in the continental shelf of China: implications for evolving anthropogenic impacts. Environ. Sci. Technol. 46, 6497–6504.

Lloyd, J., Lu, K., Liu, Z., 2024. Investigating concentrations and sources of polycyclic aromatic hydrocarbons in South and Central Texas bays and estuaries along the Gulf of Mexico, USA. Front. Mar. Sci. 11. https://doi.org/10.3389/fmars.2024.1456717.

Logan, J.M., Lutcavage, M.E., 2008. A comparison of carbon and nitrogen stable isotope ratios of fish tissues following lipid extractions with non-polar and traditional chloroform/methanol solvent systems. Rapid Commun. Mass Sp. 22, 1081–1086. https://doi.org/10.1002/rcm.3471.

Lorrain, A., Graham, B.S., Popp, B.N., Allain, V., Olson, R.J., Hunt, B.P.V., Potier, M., Fry, B., Galván-Magaña, F., Menkes, C.E.R., Kaehler, S., Ménard, F., 2015. Nitrogen isotopic baselines and implications for estimating foraging habitat and trophic position of yellowfin tuna in the Indian and Pacific Oceans. Deep-Sea Res. II Top. Stud. Oceanogr. 113, 188–198. https://doi.org/10.1016/j.dsr2.2014.02.003.

Maletić, S.P., Beljin, J.M., Rončević, S.D., Grgić, M.G., Dalmacija, B.D., 2019. State of the art and future challenges for polycyclic aromatic hydrocarbons is sediments: sources, fate, bioavailability and remediation techniques. J. Hazard. Mater. 365, 467–482. https://doi.org/10.1016/j.jhazmat.2018.11.020.

Mali, M., Di Leo, A., Giandomenico, S., Spada, L., Cardellicchio, N., Calò, M., Fedele, A., Ferraro, L., Milia, A., Renzi, M., Massara, F., Granata, T., Moruzzi, L., Buonocunto, F. P., 2022. Multivariate tools to investigate the spatial contaminant distribution in a highly anthropized area (Gulf of Naples, Italy). Environ. Sci. Pollut. R. 29, 62281–62298. https://doi.org/10.1007/s11356-022-19989-z.

Moon, K.J., Han, J.S., Ghim, Y.S., Kim, Y.J., 2008. Source apportionment of fine carbonaceous particles by positive matrix factorization at Gosan background site in East Asia. Environ. Int. 34, 654–664. https://doi.org/10.1016/j.envint.2007.12.021.

Na, G., Liang, Y., Li, R., Gao, H., Jin, S., 2021. Flux of polynuclear aromatic compounds (PAHs) from the atmosphere and from reindeer/bird feces to Arctic soils in Ny-Ålesund (Svalbard). Arch. Environ. Con. Tox. 81, 166–181. https://doi.org/10.1007/s00244-021-00851-1.

Neff, J., 1979. Polycyclic Aromatic Hydrocarbons Sources Fates and Biological Effects. Applied Science Publ, London, p. 262.

Nisbet, C., Lagoy, P., 1992. Toxic equivalency factors (TEFs) for polycyclic aromatic hydrocarbons (PAHs). Regul. Toxicol. Pharmacol. 16, 290–300. https://doi.org/10.1016/0273-2300(92)90009-X.

Park, M.-K., Cho, H.-K., Cho, I.-G., Lee, S.-E., Choi, S.-D., 2021. Contamination characteristics of polychlorinated naphthalenes in the agricultural soil of two industrial cities in South Korea. Chemosphere 273, 129721. https://doi.org/10.1016/j.chemosphere.2021.129721.

Park, Y., Kang, N., Yi, B., Lee, G., Yoo, D., 2022. Tectonostratigraphic framework in the eastern Korean continental margin, East Sea: implication for evolution of the Hupo Basin. Basin Res. 34, 797–823. https://doi.org/10.1111/bre.12641.

Ravindra, K., Sokhi, R., Van Grieken, R., 2008. Atmospheric polycyclic aromatic hydrocarbons: source attribution, emission factors and regulation. Atmos. Environ. 42, 2895–2921. https://doi.org/10.1016/j.atmosenv.2007.12.010.

Rockne, K.J., Shor, L.M., Young, L.Y., Taghon, G.L., Kosson, D.S., 2002. Distributed sequestration and release of PAHs in weathered sediment: the role of sediment structure and organic carbon properties. Environ. Sci. Technol. 36, 2636–2644. https://doi.org/10.1021/es015652h.

Shen, H., Huang, Y., Wang, R., Zhu, D., Li, W., Shen, G., Wang, B., Zhang, Y., Chen, Y., Lu, Y., Chen, H., Li, T., Sun, K., Li, B., Liu, W., Liu, J., Tao, S., 2013. Global atmospheric emissions of polycyclic aromatic hydrocarbons from 1960 to 2008 and future predictions. Environ. Sci. Technol. 47, 6415–6424. https://doi.org/10.1021/es400857z.

Shin, K.-h., Ciccantell, P.S., 2009. The steel and shipbuilding industries of South Korea: rising East Asia and globalization. J. World-Syst. Res. 15, 167–192. https://doi.org/10.5195/jwsr.2009.316.

Skotvold, T., Savinov, V., 2003. Regional distribution of PCBs and presence of technical PCB mixtures in sediments from Norwegian and Russian Arctic Lakes. Sci. Total Environ. 306, 85–97. https://doi.org/10.1016/S0048-9697(02)00486-2.

Smith, L.M., Stalling, D.L., Johnson, J.L., 1984. Determination of part-per-trillion levels of polychlorinated dibenzofurans and dioxins in environmental samples. Anal. Chem. 56, 1830. https://doi.org/10.1021/ac00275a018.

Song, M.-J., Seo, Y.-J., Lee, H.-Y., 2023. The dynamic relationship between industrialization, urbanization, CO2 emissions, and transportation modes in Korea: empirical evidence from maritime and air transport. Transportation 50, 2111–2137. https://doi.org/10.1007/s11116-022-10303-x.

Song, H., Kim, T., Lee, J., Yoon, S.J., Kim, B., Kim, Y., Hong, S., Khim, J.S., 2025. Assessment of persistent toxic substances in sediments of Gyeonggi Bay, Korea: distributions, sources, and potential ecological risks. Mar. Pollut. Bull. 213, 117652. https://doi.org/10.1016/j.marpolbul.2025.117652.

US EPA, 1993. Privisional Guidance for Quantitative Risk Assessment of Polycyclic Aromatic Hydrocarbons. US Environmental Protection Agency, Research Triangle Park, NC. EPA-600/R-93/089.

Verbruggen, E., Van Herwijnen, R., 2012. Environmental Risk Limits for Phenanthrene. RIVM Letter Report 601357007.

Villemin, D., Cherqaoui, D., Mesbah, A., 1994. Predicting carcinogenicity of polycyclic aromatic hydrocarbons from back-propagation neural network. J. Chem. Inf. Comput. Sci. 34, 1288–1293. https://doi.org/10.1021/ci00022a010.

Wang, H., Shu, Y., Kuang, Z., Han, Z., Wu, J., Huang, X., Song, X., Yang, J., Fan, Z., 2025. Bioaccumulation and potential human health risks of PAHs in marine food webs: a trophic transfer perspective. J. Hazard. Mater. 485, 136946. https://doi.org/10.1016/j.jhazmat.2024.136946.

Wania, F., Mackay, D., 1996. Peer reviewed: tracking the distribution of persistent organic pollutants. Environ. Sci. Technol. 30, 390A–396A.

Wilcke, W., 2007. Global patterns of polycyclic aromatic hydrocarbons (PAHs) in soil. Geoderma 141, 157–166. https://doi.org/10.1016/j.geoderma.2007.07.007.

Wu, Y., Zhang, J., Liu, S.M., Zhang, Z.F., Yao, Q.Z., Hong, G.H., Cooper, L., 2007. Sources and distribution of carbon within the Yangtze River system. Estuar. Coast. Shelf Sci. 71, 13–25. https://doi.org/10.1016/j.ecss.2006.08.016.

Yang, J., Sun, P., Zhang, X., Wei, X.-Y., Huang, Y.-P., Du, W.-N., Qadeer, A., Liu, M., Huang, Y., 2021. Source apportionment of PAHs in roadside agricultural soils of a megacity using positive matrix factorization receptor model and compound-specific carbon isotope analysis. J. Hazard. Mater. 403, 123592. https://doi.org/10.1016/j.jhazmat.2020.123592.

Yoo, J.H., 2017. Korea's rapid export expansion in the 1960s: how it began. KDI J. Econ. Policy Reform. 39, 1–23. https://doi.org/10.23895/kdijep.2017.39.2.1.

Yoon, S.J., Hong, S., Kwon, B.-O., Ryu, J., Lee, C.-H., Nam, J., Khim, J.S., 2017. Distributions of persistent organic contaminants in sediments and their potential impact on macrobenthic faunal community of the Geum River Estuary and Saemangeum Coast, Korea. Chemosphere 173, 216–226. https://doi.org/10.1016/j.chemosphere.2017.01.031.

Yoon, S.J., Lee, J., Kim, Y., Kwon, B.-O., Hu, W., Wang, T., Hong, S., Khim, J.S., 2025. Historical trends of polychlorinated biphenyls and alkylphenols recorded in core sediments from the intertidal areas of the Yellow Sea and Bohai Sea. Mar. Pollut. Bull. 216, 118043. https://doi.org/10.1016/j.marpolbul.2025.118043.

Zafeiraki, E., Moulas, E., Kasiotis, K.M., Bakeas, E., Dassenakis, E., 2023. Polycyclic aromatic hydrocarbons (PAHs) in surface sediments from Greece: occurrence, sources, and risk assessment. Mar. Pollut. Bull. 197, 115715. https://doi.org/10.1016/j.marpolbul.2023.115715.

Zhao, X., Jin, H., Ji, Z., Li, D., Kaw, H.Y., Chen, J., Xie, Z., Zhang, T., 2020. PAES and PAHs in the surface sediments of the East China Sea: occurrence, distribution and influence factors. Sci. Total Environ. 703, 134763. https://doi.org/10.1016/j.scitotenv.2019.134763.

<Marine Pollution Bulletin>

Supplementary materials for

Current contamination trends and historical records of traditional and emerging polycyclic aromatic hydrocarbons in sediments from Yeongil Bay and Hupo Region, East Sea

Jihyun Cha [1], Chang-Eon Lee [1], Mungi Kim, Youngnam Kim, Jiyun Gwak, Dong Jin Joe, Jae-Hyun Lim, In Kwon Um, Man Sik Choi, Seongjin Hong*

This PDF file includes:

Number of pages: 25

Number of Supplementary Tables: 10, Tables S1 to S10

Number of Supplementary Figures: 8, Figures S1 to S8

References

[1] These authors contributed equally to this work.

***Corresponding author.** *E-mail address*: hongseongjin@cnu.ac.kr (S. Hong)

Supplementary Tables

Table S1. Sampling locations and geochemical properties of surface sediments collected from Yeongil Bay, the Hupo Basin, and the Hupo Bank, East Sea.

Region	Samples	Latitude (°N)	Longitude (°E)	Water depth (m)	Mz (Phi)	TOC[a] (%)	TN[b] (%)	$\delta^{13}C$	$\delta^{15}N$	C/N ratio
Yeongil Bay	Y1	36.0405	129.4685	25	5.2	0.81	0.06	−21.3	5.8	12
	Y2	36.0402	129.4833	24	5.3	0.77	0.07	−22.6	6.4	9.4
	Y3	36.0484	129.4237	20	4.8	0.74	0.06	−21.8	5.1	11
	Y4	36.0487	129.4384	22	5.8	1.4	0.12	−24.7	5.6	9.7
	Y5	36.0487	129.4534	24	6.5	1.6	0.14	−24.6	6.0	9.8
	Y6	36.0487	129.4686	25	6.4	1.1	0.11	−23.5	5.8	8.9
	Y7	36.0577	129.4387	22	4.9	0.80	0.05	−23.2	4.2	14
	Y8	36.0575	129.4984	27	6.4	1.2	0.11	−23.6	5.9	9.3
	Y9	36.0668	129.4387	23	NA[c]	1.8	0.04	−22.4	6.7	39
	Y10	36.0663	129.4540	24	2.9	0.34	0.02	−23.0	5.2	15
	Y11	36.0660	129.4687	26	5.4	1.1	0.09	−20.2	5.4	10
	Y12	36.0666	129.4838	29	5.9	1.2	0.10	−21.8	5.4	10
	Y13	36.0665	129.4977	28	6.5	1.4	0.11	−23.3	5.0	11
	Y14	36.0759	129.4382	20	3.1	1.9	0.03	−22.1	5.7	54
	Y15	36.0758	129.4685	25	2.1	0.46	0.03	−21.6	5.9	13
	Y16	36.0850	129.4982	28	2.5	0.77	0.04	−23.1	5.5	17
	Y17	36.0937	129.4983	26	2.5	0.30	0.03	−21.4	5.4	8.7
Hupo Basin	H1	36.1710	129.5537	58	3.6	1.0	0.35	−22.2	5.1	2.5
	H2	36.3057	129.4529	79	7.8	2.0	0.25	−23.0	5.1	6.8
	H3	36.3043	129.5543	120	7.7	1.6	0.21	−21.4	5.1	6.7
	H4	36.3049	129.6458	200	9.0	2.3	0.30	−21.5	5.0	6.7
	H5	36.3037	129.7334	260	8.4	2.2	0.30	−20.8	5.1	6.2
	H6	36.3037	129.8212	410	9.7	2.5	0.31	−21.5	5.0	7.0
	H9	36.4463	129.5586	180	8.3	2.3	0.30	−22.0	5.0	6.7
	H12	36.5864	129.5980	180	8.4	1.4	0.30	−21.7	5.1	3.9
	H14	36.5808	129.8337	320	8.6	2.6	0.34	−21.7	5.0	6.6
	H15	36.6797	129.5073	80	7.9	1.5	0.16	−24.0	4.8	8.2
	H16	36.6809	129.6146	190	9.1	2.4	0.12	−22.9	5.1	18
	H18	36.6834	129.8355	330	8.3	3.3	0.35	−22.0	4.9	8.0
	H19	36.7832	129.5218	98	8.3	2.1	0.22	−23.9	4.9	8.1
	H20	36.7857	129.6325	190	8.3	2.5	0.32	−22.2	4.9	6.8
	H22	36.7851	129.8502	500	9.1	2.8	0.34	−22.4	4.8	7.0
	H23	36.8984	129.5011	125	7.7	2.1	0.23	−23.7	4.8	7.7
	H24	36.9019	129.6114	177	9.2	2.6	0.33	−22.4	4.8	6.8

	H25	36.9905	129.4880	127	7.4	2.2	0.13	−20.4	5.4	15
	H26	36.9945	129.6012	210	8.9	2.7	0.35	−22.6	4.9	6.7
	H27	36.9971	129.7110	265	7.7	2.8	0.25	−22.0	4.5	9.6
Hupo	H7	36.3843	129.7541	130	2.1	0.20	0.03	−22.3	3.7	5.7
Bank	H10	36.4483	129.6760	115	2.6	0.36	0.04	−20.2	4.4	7.7
	H11	36.4472	129.7856	146	3.6	0.68	0.06	−24.7	NA	9.7
	H13	36.5848	129.7210	110	2.8	0.46	0.05	NA	4.5	7.8
	H17	36.6814	129.7301	67	4.4	0.58	0.07	−21.8	5.6	7.2
	H21	36.7824	129.7398	133	3.2	0.40	0.05	−22.0	4.5	6.8

[a] TOC: Total organic carbon.
[b] TN: Total nitrogen.
[c] NA: Not analyed.

Table S2. Overview of core sediment properties and chronological information from the Hupo Basin, East Sea.

Samples	Latitute (°N)	Longitude (°E)	Depth (cm)	Age (Year)	Bulk density (g cm^{-3})	Sedimentation rate (cm $year^{-1}$)	TOC (%)
H8	36.4479	129.4825	0.5	2012	0.82	0.16	1.8
			4.5	1987	1.1		1.7
			6.5	1974	0.87		1.6
			8.5	1961	0.94		1.7
			11.5	1943	0.97		1.7
H15	36.6797	129.5073	0.5	2013	1.2	0.45	1.3
			2.5	2008	1.2		1.4
			4.5	2004	1.2		1.4
			6.5	1999	1.2		1.2
			8.5	1995	1.3		1.2
			10.5	1988	1.2		1.3
			14.5	1982	1.3		1.1
			17.5	1975	1.4		1.0
			20.5	1968	1.2		1.2
			24.5	1959	1.3		1.2
			28.5	1950	1.3		NA[a]
			32.5	1941	1.5		NA
H20	36.7857	129.6325	0.5	2012	1.0	0.31	2.0
			2.5	2006	0.90		2.4
			4.5	1999	0.79		2.1
			6.5	1993	0.94		2.2
			8.5	1986	0.81		2.1
			11.5	1977	0.87		2..2
			14.5	1967	0.83		2.5
			17.5	1957	0.82		2.4
			20.5	1948	0.78		2.2
H25	36.9905	129.4880	1.5	2012	1.0	0.50	NA
			3.5	2008	1.0		NA
			7.5	2000	0.98		2.0
			9.5	1996	1.1		2.1
			11.5	1992	1.1		2.0
			14.5	1986	1.1		2.4
			15.5	1980	1.0		2.2
			17.5	1974	1.1		2.2
			23.5	1968	1.1		2.2

[a] NA: Not analyed.

Table S3. Target polycyclic aromatic hydrocarbons (PAHs), surrogate standards, and instrumental parameters, including quantification and confirmation ions, retention times, limit of detection and quantification, and recoveries.

Target compounds	Abbreviation	Quantification ion	Confirmation ion	Retention times (min.)	Limit of detection (ng g^{-1} dw)	Limit of quantification (ng g^{-1} dw)
Traditional polycyclic aromatic hydrocarbons (t-PAHs)						
Acenaphthylene	Acl	152	151	12.826	0.06	0.18
Acenaphthene	Ace	153	154	13.260	0.12	0.35
Fluorene	Flu	166	165	14.473	0.15	0.44
Phenanthrene	Phe	178	176	16.768	0.06	0.18
Anthracene	Ant	178	176	16.877	0.07	0.21
Fluoranthene	Fl	202	200	20.959	0.09	0.26
Pyrene	Py	202	200	21.939	0.12	0.35
Benzo[*a*]anthracene	BaA	228	226	29.748	0.06	0.18
Chrysene	Chr	228	226	30.035	0.03	0.09
Benzo[*b*]fluoranthene	BbF	252	253	38.860	0.08	0.23
Benzo[*k*]fluoranthene	BkF	252	253	39.114	0.20	0.59
Benzo[*a*]pyrene	BaP	252	253	42.075	0.09	0.26
Indeno[*1,2,3-cd*]pyrene	IcdP	276	138	53.275	0.09	0.26
Benzo[*g,h,i*]perylene	BghiP	276	138	53.712	0.12	0.35
Dibenz[*a,h*]anthracene	DbahA	278	276	54.655	0.07	0.21
Emerging polycyclic aromatic hydrocarbons (e-PAHs)						
2-Methylanthracene	2MA	192	191	18.456	0.81	2.37
9-Ethylphenanthrene	9EP	191	206	19.953	0.06	0.18
Benzo[*b*]naphtho[*2,3-d*]furan	BBNF	219	219	22.756	0.32	0.94
11H-benzo[*b*]fluorene	11BbF	216	215	24.361	0.23	0.67
Benzo[*b*]naphtho[*2,1-d*]thiophene	BBNT	234	235	27.945	0.12	0.35
5-Methylbenz[*a*]anthracene	5MbA	242	241	34.010	0.20	0.59
1,12-dimethylbenzo[*c*]phenanthrene	BCP	256	241	34.317	0.34	1.0
Benzo[*e*]pyrene	BeP	252	250	41.543	0.28	0.82
Internal standard						
2-Fluorobiphenyl	IS	172	171	11.699		
Surrogate standards	**Abbreviation**	**Quantification ion**	**Confirmation ion**	**Retention times (min.)**	**Surrogate recovery (%, mean ± SD)**	
Acenaphthene-d10	Ace-d10	164	162	13.260	73 ± 13	
Phenanthrene-d10	Phe-d10	188	189	16.769	75 ± 8.0	
Chrysene-d12	Chr-d12	240	236	30.015	87 ± 12	
Perylene-d12	Per-d12	264	270	53.459	88 ± 11	

Table S4. GC-MSD instrumental conditions for the analysis of t-PAHs and e-PAHs in sediments.

Instrument	GC: Agilent Technologies 7890B, MSD: Agilent Technologies 5977B
Samples	F2 from sediment extracts
Analytical column	DB-5MS (30 m × 0.25 mm i.d. × 0.25 μm film)
Carrier gas	Helium
Injection volume	1.0 μL
Flow rate	1.0 mL min^{-1}
Mass range	50–600 *m/z*
Ion source temperature	230 ℃
Ionization mode	EI mode (70 eV)
Oven temperature	60 ℃ (hold 2 min) → 6 ℃ min^{-1} to 300 ℃ (hold 13 min)

Table S5. Predicted no-effect concentrations (PNECs) of 23 PAHs in sediments estimated using the ecological structure-activity relationships (ECOSAR) model.

Compounds	Organism	Endpoint	Duration	Value (mg L^{-1})	Assessment factor	Log K_{OW}	$K_{sus\text{-}water}$	PNEC (sediment, ng g^{-1})
t-PAHs								
Acl				2.4		3.9	0.83	1700
Ace				1.7		3.9	0.82	1200
Flu				2.3		4.2	0.88	1800
Phe				1.5		4.5	0.94	1200
Ant				1.5		4.5	0.93	1200
Fl				0.66		5.2	1.1	620
Py				0.66		4.9	1.0	580
BaA	Green Algae	EC_{50}	96h	0.29	1000	5.8	1.2	310
Chr				0.29		5.8	1.2	310
BbF				0.13		5.8	1.2	130
BkF				0.13		6.1	1.3	140
BaP				0.13		6.1	1.3	140
IcdP				0.05		6.7	1.4	66
BghiP				0.05		6.5	1.4	65
DbahA				0.05		6.5	1.4	65
e-PAHs								
2MA				0.67		4.9	1.0	590
9EP				0.33		5.4	1.1	320
BBNF				0.76		4.9	1.0	680
11BbF	Green Algae	EC_{50}	96h	0.46	1000	5.8	1.2	490
BBNT				0.40		5.2	1.1	380
5MbA				0.13		6.1	1.3	140
BCP				0.06		6.6	1.4	69
BeP				0.13		6.1	1.3	140

Table S6. Toxic equivalency factors (TEFs) and mutagenic equivalency factors (MEFs) used for calculating carcinogenic and mutagenic potencies of target PAHs.

Target compounds	TEF value	Reference	MEF value	Reference
BaA	0.10	Nisbet and LaGoy (1992)	0.08	Durant et al. (1996, 1999)
Chr	0.01		0.02	
BbF	0.10		0.25	
BkF	0.10		0.11	
BaP	1.0		1.0	
IcdP	0.10		0.31	
DbahA	1.0	EPA (1993)	0.29	
BghiP	0.01	Nisbet and LaGoy (1992)	1.9	

Table S7. Concentrations of PAHs in surface sediments from Yeongil Bay, the Hupo Basin, and the Hupo Bank, East Sea.

Region	Samples	Concentrations of PAHs (ng g^{-1} dm)							
		Acl	**Ace**	**Flu**	**Phe**	**Ant**	**Fl**	**BBNF**	**11BbF**
Yeongil Bay	Y1	1.4	8.0	9.2	43	3.3	83	3.2	ND
	Y2	1.4	7.4	9.0	38	4.0	63	2.5	ND
	Y3	0.69	ND	1.8	6.0	1.1	31	1.9	ND
	Y4	ND[a]	70	14	59	54	ND	120	63
	Y5	4.4	32	25	92	13	160	7.6	ND
	Y6	ND	34	2.7	29	19	ND	35	66
	Y7	ND	12	8.3	25	2.2	26	ND	ND
	Y8	3.3	23	25	100	12	160	7.2	ND
	Y9	1.7	5.5	ND	16	2.3	59	3.2	ND
	Y10	ND	5.1	ND	8.4	0.81	8.1	ND	ND
	Y11	1.9	8.8	ND	46	5.4	69	3.0	ND
	Y12	1.2	1.8	ND	12	1.3	14	ND	ND
	Y13	6.4	41	45	190	26	340	16	ND
	Y14	ND	ND	ND	9.9	0.92	13	ND	ND
	Y15	ND	4.1	ND	32	3.5	48	2.7	ND
	Y16	2.8	17	ND	90	11	140	6.6	ND
	Y17	ND	ND	2.0	3.1	0.44	1.0	ND	ND
Hupo Basin	H1	3.5	4.4	ND	29	2.7	22	2.1	ND
	H2	ND	ND	ND	29	2.8	26	2.7	ND
	H3	ND	ND	ND	23	1.6	9.4	ND	ND
	H4	ND	ND	ND	28	2.7	22	3.6	ND
	H5	ND	ND	ND	110	11	86	14	ND
	H6	ND	5.3	ND	47	3.6	38	3.0	ND
	H9	ND	3.2	ND	7.9	0.72	3.6	0.92	ND
	H12	1.7	3.1	ND	19	ND	13	ND	ND
	H14	ND	3.4	ND	16	ND	9.0	ND	ND
	H15	ND	6.9	ND	14	1.50	18	1.7	ND
	H16	ND	2.1	8.4	7.7	ND	5.1	ND	ND
	H18	ND	3.4	ND	16	ND	9.0	ND	ND
	H19	ND	11	ND	23	2.2	22	ND	ND
	H20	1.0	6.5	7.6	19	19	24	1.6	ND
	H22	ND	11	ND	26	2.1	29	2.3	ND
	H23	ND	11	ND	23	2.1	28	2.2	ND
	H24	ND	11	ND	26	2.2	34	2.6	ND
	H25	ND	2.3	ND	21	2.7	24	2.2	ND
	H26	1.5	7.0	10	28	2.8	32	2.5	ND
	H27	1.6	7.7	ND	28	2.2	29	2.3	ND
Hupo Bank	H7	ND	3.3	ND	35	2.9	27	2.4	ND
	H10	ND	2.9	ND	22	1.9	20	2.0	ND
	H11	1.6	3.5	ND	7.6	0.73	4.6	1.0	ND
	H13	0.47	ND	ND	9.4	0.82	9.4	0.72	ND
	H17	ND	3.4	ND	16	ND	9.0	ND	ND
	H21	ND	8.7	5.7	8.8	0.72	5.0	ND	ND

Table S7. (Continued)

Region	Samples	Concentrations of PAHs (ng g^{-1} dm)							
		BBNT	2MA	9EP	Py	BaA	Chr	BbF	BkF
Yeongil Bay	Y1	2.9	ND	2.6	130	30	19	28	17
	Y2	2.8	1.5	ND	120	22	14	20	13
	Y3	5.0	ND	1.9	29	13	15	19	10
	Y4	ND	12	ND	58	9.2	55	ND	ND
	Y5	8.6	3.5	7.0	230	73	45	61	45
	Y6	ND	7.9	ND	24	8.4	29	ND	ND
	Y7	0.31	1.5	2.0	71	5.5	4.9	3.8	2.8
	Y8	7.7	3.1	7.1	220	70	42	61	40
	Y9	0.89	1.6	1.4	70	27	15	16	12
	Y10	ND	ND	0.72	23	ND	2.3	0.92	0.56
	Y11	3.5	1.8	2.5	120	28	18	23	15
	Y12	0.09	ND	1.1	36	4.7	4.1	2.5	1.6
	Y13	20	6.4	11	450	170	94	140	94
	Y14	ND	ND	0.92	41	ND	2.4	0.92	0.48
	Y15	1.0	2.6	2.6	130	14	10	9.1	5.9
	Y16	9.4	3.4	5.8	210	62	39	54	35
	Y17	ND	ND	0.45	0.85	ND	1.8	0.16	ND
Hupo Basin	H1	0.68	1.5	1.6	16	8.8	7.7	13	7.4
	H2	1.0	ND	2.8	23	11	11	11	8.5
	H3	ND	ND	1.9	9.5	ND	ND	1.3	0.75
	H4	ND	ND	3.5	21	10	11	3.5	3.8
	H5	ND	ND	14	86	41	44	26	15
	H6	1.0	1.8	4.1	32	13	12	23	14
	H9	ND	1.1	0.71	3.6	2.6	2.5	1.7	0.73
	H12	ND	3.2	5.9	12	ND	3.0	ND	ND
	H14	ND	1.2	1.5	7.2	3.2	3.5	3.8	2.1
	H15	0.64	ND	1.7	17	8.8	7.0	8.0	5.1
	H16	ND	1.1	0.90	5.4	2.6	2.7	2.4	12
	H18	ND	1.2	1.5	7.2	3.2	3.5	3.8	2.1
	H19	0.46	ND	ND	19	9.8	8.4	9.6	6.1
	H20	0.72	0.81	2.1	18	7.2	8.0	12	7.0
	H22	0.25	ND	2.6	24	9.1	10	15	8.6
	H23	0.30	ND	2.4	19	8.8	9.1	12	6.6
	H24	0.56	ND	3.2	26	11	11	17	10
	H25	1.0	1.5	2.4	22	15	14	32	21
	H26	0.64	1.5	3.0	25	11	13	22	12
	H27	0.38	ND	3.1	22	9.0	10	16	9.4
Hupo Bank	H7	0.41	1.7	3.4	25	11	9.8	17	10
	H10	ND	1.5	2.2	18	7.2	6.4	9.1	5.6
	H11	ND	1.1	0.89	4.2	2.8	2.8	2.3	1.2
	H13	0.32	ND	1.1	11	2.8	3.2	3.8	2.6
	H17	ND	1.2	1.5	7.2	3.2	3.5	3.8	2.1
	H21	ND	ND	0.86	4.0	2.6	2.9	1.5	0.81

Table S7. (Continued)

Region	Samples	Concentrations of PAHs (ng g^{-1} dm)							
		5MbA	BCP	BeP	BaP	IcdP	DbahA	BghiP	SUM
Yeongil Bay	Y1	ND	ND	ND	ND	35	6.9	36	460
	Y2	ND	ND	ND	ND	26	5.5	26	380
	Y3	ND	ND	ND	ND	17	ND	18	170
	Y4	18	8.2	17	ND	ND	23	19	600
	Y5	ND	ND	ND	34	69	9.6	81	1000
	Y6	14	8.2	14	ND	ND	20	18	330
	Y7	ND	ND	ND	13	ND	ND	ND	180
	Y8	ND	ND	ND	67	76	14	78	1000
	Y9	ND	ND	ND	22	21	ND	21	300
	Y10	ND	ND	ND	13	ND	ND	ND	63
	Y11	ND	ND	ND	25	30	6.1	30	440
	Y12	ND	ND	ND	13	ND	ND	ND	93
	Y13	ND	ND	ND	26	180	34	170	2100
	Y14	ND	ND	ND	13	ND	ND	ND	83
	Y15	ND	ND	ND	ND	13	ND	14	290
	Y16	ND	ND	ND	14	67	14	68	850
	Y17	ND	ND	ND	40	ND	ND	ND	50
Hupo Basin	H1	1.9	0.93	11	10	17	3.8	15	180
	H2	ND	ND	ND	ND	13	ND	15	160
	H3	ND	ND	ND	ND	ND	ND	ND	48
	H4	ND	ND	ND	ND	ND	ND	ND	110
	H5	ND	ND	ND	ND	ND	ND	ND	450
	H6	1.7	0.93	20	15	28	4.5	23	290
	H9	1.1	0.93	2.2	2.2	3.1	1.7	2.4	43
	H12	1.1	0.93	ND	ND	ND	ND	ND	63
	H14	1.1	0.93	ND	ND	4.8	ND	4.8	63
	H15	ND	ND	ND	ND	11	ND	11	110
	H16	1.1	0.90	ND	ND	5.1	ND	3.2	50
	H18	1.1	0.93	ND	ND	4.8	ND	4.8	63
	H19	ND	ND	ND	ND	13	ND	12	140
	H20	0.66	0.67	ND	ND	19	2.6	18	180
	H22	ND	ND	ND	ND	25	ND	22	190
	H23	ND	ND	ND	ND	18	ND	18	160
	H24	ND	ND	ND	ND	26	ND	24	200
	H25	1.4	0.93	32	43	46	10	45	340
	H26	ND	ND	ND	ND	31	ND	28	230
	H27	ND	ND	ND	ND	25	ND	22	190
Hupo Bank	H7	1.6	0.93	15	12	22	4.2	20	220
	H10	1.3	0.93	7.9	7.5	12	2.9	10	140
	H11	1.2	0.93	2.6	2.5	3.9	ND	3.0	49
	H13	ND	ND	ND	ND	4.5	ND	4.9	55
	H17	1.1	0.93	ND	ND	4.8	ND	4.8	63
	H21	ND	ND	ND	ND	ND	ND	ND	42

[a] ND: Not detected.

Table S8. BaP-TEQ (carcinogenic equivalents, ng g^{-1} dm) concentrations of PAHs in surface sediments from Yeongil Bay, the Hupo Basin, and the Hupo Bank, East Sea.

Region	Samples	BaP-TEQ (ng g^{-1} dm)								
		BaA	**Chr**	**BbF**	**BkF**	**BaP**	**IcdP**	**DbahA**	**BghiP**	**SUM**
Yeongil Bay	Y1	3.0	0.19	2.8	1.7	ND[a]	3.5	6.9	0.36	18
	Y2	2.2	0.14	2.0	1.3	ND	2.6	5.5	0.26	14
	Y3	1.3	0.15	1.9	1.0	ND	1.7	ND	0.18	6.2
	Y4	0.92	0.55	ND	ND	ND	ND	23	0.19	25
	Y5	7.3	0.45	6.1	4.5	34	6.9	9.6	0.81	70
	Y6	0.84	0.29	ND	ND	ND	ND	20	0.18	21
	Y7	0.55	0.05	0.38	0.28	13	ND	ND	ND	14
	Y8	7.0	0.42	6.1	4.0	67	7.6	14	0.78	110
	Y9	2.7	0.15	1.6	1.2	22	2.1	ND	0.21	30
	Y10	ND	0.02	0.09	0.06	13	ND	ND	ND	13
	Y11	2.8	1.18	2.3	1.5	25	3.0	6.1	0.30	41
	Y12	0.47	0.04	0.25	0.16	13	ND	ND	ND	14
	Y13	17	0.94	14	9.4	26	18	34	1.7	120
	Y14	ND	0.02	0.09	0.05	13	ND	ND	ND	13
	Y15	1.4	0.10	0.91	0.59	ND	1.3	ND	0.14	4.4
	Y16	6.2	0.39	5.4	3.5	14	6.7	14	0.68	51
	Y17	ND	0.02	0.02	ND	40	ND	ND	ND	40
Hupo Basin	H1	0.88	0.08	1.3	0.74	10	1.7	3.8	0.15	19
	H2	1.1	0.11	1.1	0.85	ND	1.3	ND	0.15	4.6
	H3	ND	ND	0.13	0.08	ND	ND	ND	ND	0.21
	H4	1.0	0.11	0.65	0.38	ND	ND	ND	ND	2.2
	H5	4.1	0.44	2.6	1.5	ND	ND	ND	ND	8.6
	H6	1.3	0.12	2.3	1.4	15	2.8	4.5	0.23	28
	H9	0.26	0.03	0.17	0.07	2.2	0.31	1.7	0.02	4.8
	H12	ND	0.03	ND	ND	ND	ND	ND	ND	0.03
	H14	0.32	0.04	0.38	0.21	ND	0.48	ND	0.05	1.5
	H15	0.88	0.07	0.80	0.51	ND	1.1	ND	0.11	3.5
	H16	0.26	0.03	0.24	0.12	ND	0.51	ND	0.03	1.2
	H18	0.32	0.04	0.38	0.21	ND	0.48	ND	0.05	1.5
	H19	0.98	0.08	0.96	0.61	ND	1.3	ND	0.12	4.1
	H20	0.72	0.08	1.2	0.70	ND	1.9	2.6	0.18	7.4
	H22	0.91	0.10	1.5	0.86	ND	2.5	ND	0.22	6.1
	H23	0.88	0.09	1.2	0.66	ND	1.8	ND	0.18	4.8
	H24	1.1	0.11	1.7	1.0	ND	2.6	ND	0.24	6.8
	H25	1.5	0.14	3.2	2.1	43	4.6	10	0.45	65
	H26	1.1	0.13	2.2	1.2	ND	3.1	ND	0.28	8.0
	H27	0.90	0.10	1.6	0.94	ND	2.5	ND	0.22	6.3
Hupo Bank	H7	1.1	0.10	1.7	1.0	12	2.2	4.5	0.20	23
	H10	0.72	0.06	0.91	0.56	7.5	1.2	2.9	0.10	14
	H11	0.28	0.03	0.23	0.12	2.5	0.39	ND	0.03	3.6
	H13	0.28	0.03	0.38	0.26	ND	0.45	ND	0.05	1.5
	H17	0.32	0.04	0.38	0.21	ND	0.48	ND	0.05	1.5
	H21	0.26	0.03	0.15	0.08	ND	ND	ND	ND	0.52

[a] ND: Not detected.

Table S9. BaP-MEQ (mutagenic equivalents, ng g^{-1} dm) concentrations of PAHs in surface sediments from Yeongil Bay, the Hupo Basin, and the Hupo Bank, East Sea.

Region	Samples	BaP-MEQ (ng g^{-1} dm)								
		BaA	**Chr**	**BbF**	**BkF**	**BaP**	**IcdP**	**DbahA**	**BghiP**	**SUM**
Yeongil Bay	Y1	2.5	0.32	7.0	1.9	ND[a]	11	2.0	6.8	31
	Y2	1.8	0.24	5.0	1.4	ND	8.1	1.6	4.9	23
	Y3	1.1	0.26	4.8	1.1	ND	5.3	ND	3.4	16
	Y4	0.75	0.94	ND	ND	ND	ND	6.7	3.6	12
	Y5	6.0	0.77	15	4.9	34	21	2.8	15	100
	Y6	0.69	0.49	ND	ND	ND	ND	5.8	3.4	10
	Y7	0.45	0.08	0.95	0.31	13	ND	ND	ND	15
	Y8	5.7	0.71	15	4.4	67	24	4.1	15	140
	Y9	2.2	0.26	4.0	1.3	22	6.5	ND	4.0	40
	Y10	ND	0.04	0.23	0.06	13	ND	ND	ND	13
	Y11	2.3	0.31	5.8	1.7	25	9.3	1.8	5.7	52
	Y12	0.39	0.07	0.63	0.18	13	ND	ND	ND	14
	Y13	14	1.6	35	10	26	56	9.9	32	180
	Y14	ND	0.04	0.23	0.05	13	ND	ND	ND	13
	Y15	1.2	0.17	2.3	0.65	ND	4.0	ND	2.7	11
	Y16	5.1	0.66	14	3.9	14	21	4.1	13	75
	Y17	ND	0.03	0.04	ND	40	ND	ND	ND	40
Hupo Basin	H1	0.72	0.13	3.3	0.81	10	5.3	1.1	2.9	24
	H2	0.90	0.19	2.8	0.94	ND	4.0	ND	2.9	12
	H3	ND	ND	0.33	0.08	ND	ND	ND	ND	0.41
	H4	0.84	0.19	1.6	0.41	ND	ND	ND	ND	3.1
	H5	3.4	0.75	6.5	1.7	ND	ND	ND	ND	12
	H6	1.1	0.20	5.8	1.5	15	8.7	1.3	4.4	38
	H9	0.21	0.04	0.43	0.08	2.2	0.96	0.49	0.46	4.9
	H12	ND	0.05	ND	ND	ND	ND	ND	ND	0.05
	H14	0.26	0.06	0.95	0.23	ND	1.5	ND	0.91	3.9
	H15	0.72	0.12	2.0	0.56	ND	3.4	ND	2.1	8.9
	H16	0.21	0.05	0.60	0.13	ND	1.6	ND	0.61	3.2
	H18	0.26	0.06	0.95	0.23	ND	1.5	ND	0.91	3.9
	H19	0.80	0.14	2.4	0.67	ND	4.0	ND	2.3	10
	H20	0.59	0.14	3.0	0.77	ND	5.9	0.75	3.4	15
	H22	0.75	0.17	3.8	0.95	ND	7.8	ND	4.2	18
	H23	0.72	0.15	3.0	0.73	ND	5.6	ND	3.4	14
	H24	0.90	0.19	4.3	1.1	ND	8.1	ND	4.6	19
	H25	132	0.24	8.0	2.3	43	14	2.9	8.6	80
	H26	0.90	0.22	5.5	1.3	ND	9.6	ND	5.3	23
	H27	0.74	0.17	4.0	1.0	ND	7.8	ND	4.2	18
Hupo Bank	H7	0.90	0.17	4.3	1.1	12	6.8	1.2	3.8	30
	H10	0.59	0.11	2.3	0.62	7.5	3.7	0.84	1.9	18
	H11	0.23	0.05	0.58	0.13	2.5	1.2	ND	0.57	5.3
	H13	0.23	0.05	0.95	0.29	ND	1.4	ND	0.93	3.9
	H17	0.26	0.06	0.94	0.24	ND	1.5	ND	0.91	3.9
	H21	0.21	0.05	0.38	0.09	ND	ND	ND	ND	0.73

[a] ND: Not detected.

Table S10. Concentrations of PAHs in core sediments from the Hupo Basin, East Sea.

Samples	Age (yr)	Concentrations of PAHs (ng g^{-1} dm)							
		Acl	Ace	Flu	Phe	Ant	Fl	BBNF	11BbF
H8	2012	ND[a]	2.2	11	32	2.7	39	3..0	ND
	1987	1.6	ND	9.6	29	2.2	30	2.6	ND
	1974	1.7	ND	7.3	31	3.6	59	3.5	ND
	1961	1.4	1.4	6.9	25	2.1	32	2.6	ND
	1943	ND	ND	15	37	4.6	35	7.4	ND
H15	2013	ND	ND	ND	17	1.5	26	2.0	ND
	2008	ND	ND	ND	14	1.7	21	2.0	ND
	2004	ND	ND	ND	13	1.8	22	2.0	ND
	1999	ND	2.2	ND	13	2.0	27	2.3	ND
	1995	1.4	ND	4.4	17	1.6	20	1.8	ND
	1988	ND	ND	ND	17	1.6	23	1.8	ND
	1982	ND	1.1	4.1	15	1.4	17	1.7	ND
	1975	ND	ND	4.7	15	1.3	14	1.5	ND
	1968	ND	ND	ND	8.4	0.63	3.2	0.90	ND
	1959	ND	ND	ND	13	0.86	5.1	ND	ND
	1950	ND	ND	ND	11	0.77	4.3	ND	ND
	1941	ND	ND	ND	10	0.77	3.4	ND	ND
H20	2012	ND	ND	ND	17	5.6	12	ND	ND
	2006	ND	ND	ND	23	7.9	21	5.8	ND
	1999	ND	ND	ND	28	4.2	26	5.9	ND
	1993	ND	ND	ND	25	5.4	24	8.4	ND
	1986	4.4	ND	ND	20	3.9	21	ND	ND
	1977	ND	ND	ND	20	3.3	17	5.3	ND
	1967	ND	ND	7.3	18	3.3	16	5.2	ND
	1957	NA[b]	NA	NA	NA	NA	NA	NA	NA
	1948	NA	NA	NA	NA	NA	NA	NA	NA
H25	2012	ND	8.9	ND	25	2.1	21	3.2	ND
	2008	ND	8.9	7.9	18	2.0	16	2.9	ND
	2000	ND	11	ND	19	2.2	ND	ND	ND
	1996	ND	10	7.0	17	2.0	15	ND	ND
	1992	ND	ND	ND	ND	ND	ND	ND	ND
	1986	ND	3.5	2.5	5.5	0.64	ND	ND	ND
	1980	ND	7.5	ND	11	1.3	10	ND	ND
	1974	ND	6.4	4.6	10	1.1	8.0	ND	ND
	1968	ND	ND	3.5	13	1.0	8.4	1.2	ND

Table S10. (Continued)

Samples	Age (yr)	Concentrations of PAHs (ng g^{-1} dm) BBNT	2MA	9EP	Py	BaA	Chr	BbF	BkF
H8	2012	0.93	ND	2.7	27	14	12	15	7.8
	1987	0.44	ND	1.8	20	10	8.8	10	5.3
	1974	1.4	1.6	1.8	44	22	15	20	12
	1961	0.66	ND	1.9	22	12	10	14	7.6
	1943	ND	ND	ND	26	23	3.0	14	7.4
H15	2013	ND	ND	1.5	23	7.5	7.5	7.5	7.1
	2008	0.30	1.3	1.5	16	9.8	7.8	9.3	6.5
	2004	0.30	ND	ND	18	9.8	7.4	8.9	6.4
	1999	0.45	1.4	1.5	21	12	8.4	11	7.6
	1995	0.23	1.3	1.2	15	9.2	6.8	7.7	5.8
	1988	0.25	ND	1.3	21	9.0	6.8	7.6	5.0
	1982	0.21	1.2	1.1	13	7.9	5.9	6.5	4.4
	1975	0.07	ND	1.0	11	6.7	5.3	5.3	3.6
	1968	ND	ND	0.66	3.0	2.1	2.2	0.92	0.47
	1959	ND	ND	0.85	5.0	ND	2.6	1.5	0.82
	1950	ND	ND	0.84	4.5	2.3	2.4	1.1	0.58
	1941	ND	ND	0.70	3.0	ND	2.3	1.0	0.56
H20	2012	ND	ND	ND	12	22	17	8.4	4.0
	2006	ND	ND	ND	17	19	15	12	7.0
	1999	ND	ND	ND	18	21	17	21	11
	1993	ND	ND	ND	25	30	22	18	9.6
	1986	ND	ND	ND	18	21	16	18	9.9
	1977	ND	ND	ND	13	19	14	13	7.6
	1967	ND	ND	ND	12	20	14	15	8.1
	1957	NA	NA	NA	NA	NA	NA	NA	NA
	1948	NA	NA	NA	NA	NA	NA	NA	NA
H25	2012	ND	ND	ND	16	9.3	9.0	7.3	3.8
	2008	ND	ND	ND	12	8.6	7.9	6.6	3.6
	2000	ND	ND	ND	12	8.4	7.8	6.7	3.3
	1996	ND	ND	ND	12	8.3	7.3	5.1	2.6
	1992	ND	ND	ND	ND	ND	ND	ND	ND
	1986	ND	ND	ND	3.1	2.5	2.4	1.8	0.91
	1980	ND	ND	ND	6.7	5.5	5.0	3.7	1.9
	1974	ND	ND	ND	5.4	5.1	4.6	2.8	1.6
	1968	ND	ND	1.2	6.0	ND	3.5	3.2	2.2

Table S10. (Continued)

Samples	Age (yr)	Concentrations of PAHs (ng g^{-1} dm) 5MbA	BCP	BeP	BaP	IcdP	DbahA	BghiP	SUM
H8	2012	ND	ND	ND	ND	24	ND	22	220
	1987	ND	ND	ND	ND	20	ND	19	170
	1974	ND	ND	ND	ND	34	ND	32	290
	1961	ND	ND	ND	ND	22	4.0	20	190
	1943	ND	ND	19	23	35	ND	29	280
H15	2013	ND	ND	ND	ND	9.0	ND	11	120
	2008	ND	ND	ND	ND	11	ND	12	110
	2004	ND	ND	ND	ND	11	ND	11	110
	1999	ND	ND	ND	ND	13	ND	13	140
	1995	ND	ND	ND	ND	10	ND	10	110
	1988	ND	ND	ND	ND	8.8	ND	8.5	110
	1982	ND	ND	ND	ND	8.8	ND	7.8	97
	1975	ND	ND	ND	ND	7.3	ND	6.7	84
	1968	ND	ND	ND	ND	ND	ND	ND	23
	1959	ND	ND	ND	ND	ND	ND	ND	30
	1950	ND	ND	ND	ND	ND	ND	ND	28
	1941	ND	ND	ND	ND	ND	ND	ND	22
H20	2012	ND	ND	14	16	21	ND	14	160
	2006	ND	ND	16	16	23	ND	19	200
	1999	ND	ND	22	20	35	ND	28	260
	1993	ND	ND	23	25	34	ND	23	270
	1986	ND	ND	20	21	32	ND	25	230
	1977	ND	ND	16	17	25	ND	17	190
	1967	ND	ND	17	17	25	ND	18	190
	1957	NA	NA	NA	NA	NA	NA	NA	NA
	1948	NA	NA	NA	NA	NA	NA	NA	NA
H25	2012	ND	ND	8.3	8.2	ND	ND	ND	120
	2008	ND	ND	7.9	8.5	11	ND	ND	120
	2000	ND	ND	8.5	9.0	11	ND	ND	99
	1996	ND	ND	6.8	7.9	8.8	ND	6.5	120
	1992	ND	ND	ND	ND	ND	ND	ND	ND
	1986	ND	ND	2.3	2.4	3.2	ND	ND	31
	1980	ND	ND	4.7	4.9	6.5	ND	ND	69
	1974	ND	ND	4.4	5.2	5.7	ND	ND	65
	1968	ND	ND	ND	ND	5.2	1.7	4.3	54

[a] ND: Not detected.
[b] NA: Not analyzed.

Supplementary Figures

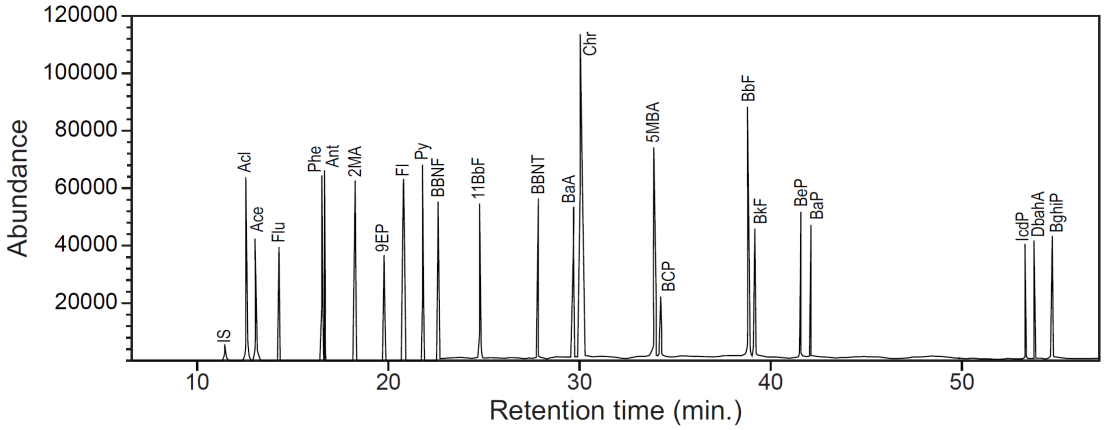

Fig. S1. GC-MSD chromatogram of the 23 PAHs analyzed in this study.

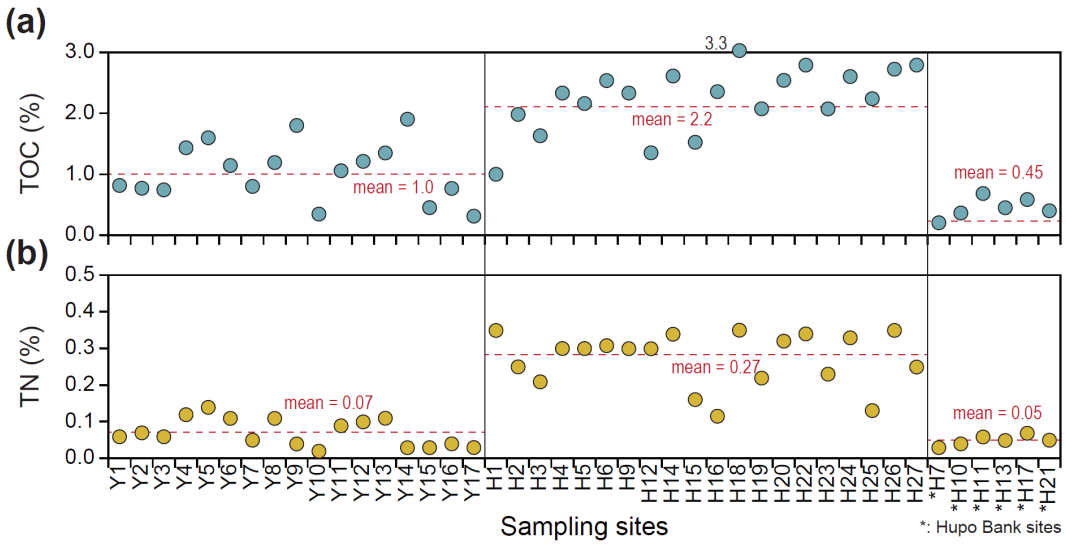

Fig. S2. (a) Total organic carbon (TOC, %) and **(b)** total nitrogen (TN, %) contents in surface sediments from Yeongil Bay, the Hupo Basin, and the Hupo Bank, East Sea. Sampling sites in the Hupo Bank are marked with asterisks (*).

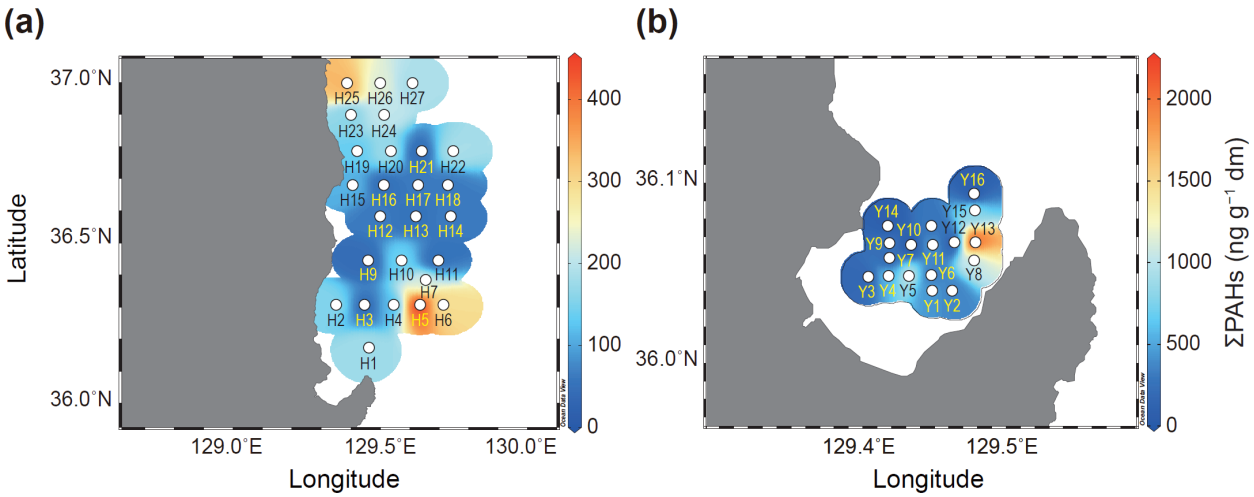

Fig. S3. Spatial distribution of ΣPAHs (ng g^{-1} dm) in surface sediments from **(a)** the Hupo Basin and the Hupo Bank and **(b)** Yeongil Bay. Spatial interpolation of PAHs was estimated using Ocean Data View (ODV) software.

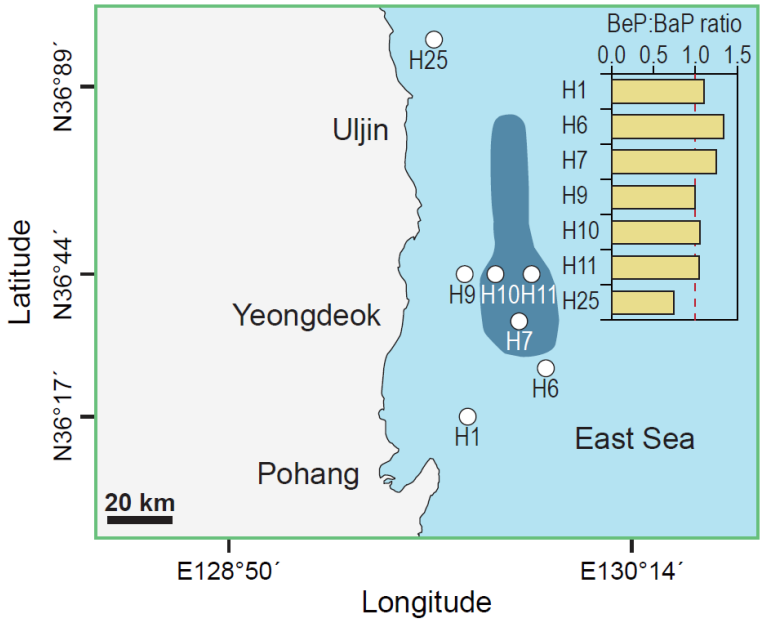

Fig. S4. Spatial distribution of the benzo[*e*]pyrene to benzo[*a*]pyrene (BeP/BaP) ratio in surface sediments from the Hupo Basin, East Sea. This BeP:BaP ratio is commonly used to assess photochemical degradation during atmospheric transport (Lee et al., 2001, 2006).

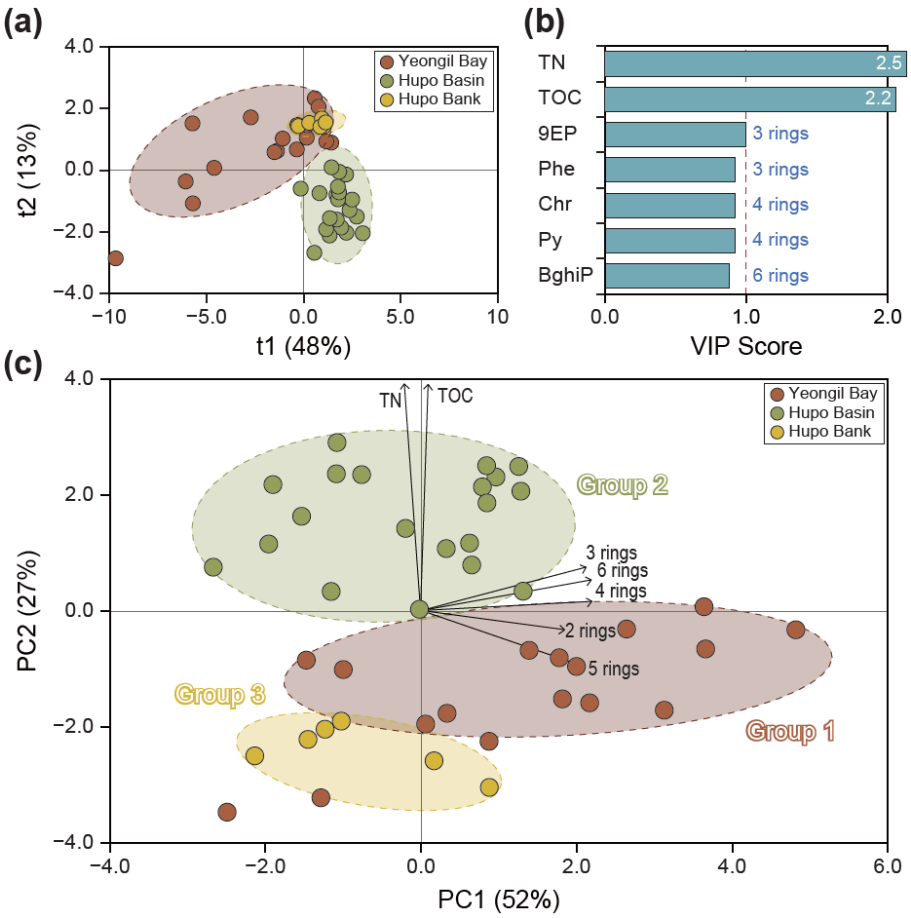

Fig. S5. (a) Partial least squares (PLS) analysis based on TOC, TN, and PAH concentrations in surface sediments from Yeongil Bay, the Hupo Basin, and the Hupo Bank. **(b)** Variable importance in projection (VIP) scores derived from the PLS model. Variables with VIP > 1.0 were considered significant contributors to site discrimination; selected PAHs are labeled by ring number. **(c)** Principal component analysis (PCA) results based on TOC, TN, and PAH concentrations. Arrows indicate loading vectors, where direction represents correlation with principal components and length shows the relative contribution of each variable.

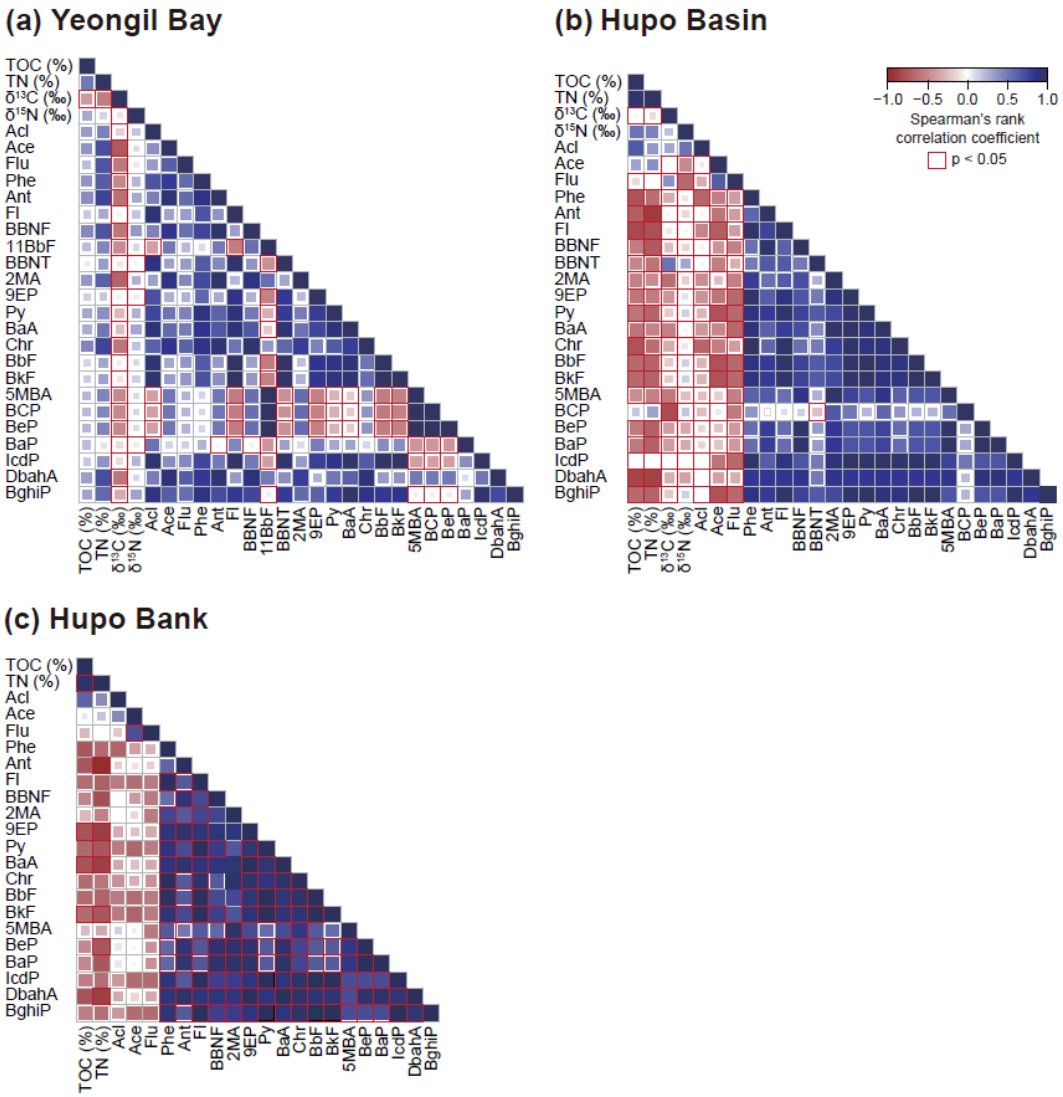

Fig. S6. Spearman rank correlation analysis between sediment properties (TOC, TN, $\delta^{13}C$, and $\delta^{15}N$) and concentrations of individual PAHs in surface sediments from **(a)** Yeongil Bay, **(b)** the Hupo Basin, and **(c)** the Hupo Bank, East Sea. Color gradients indicate the strength and direction of positive (blue) and negative (red) correlations. Red boxes highlight statistically significant correlations ($p < 0.05$).

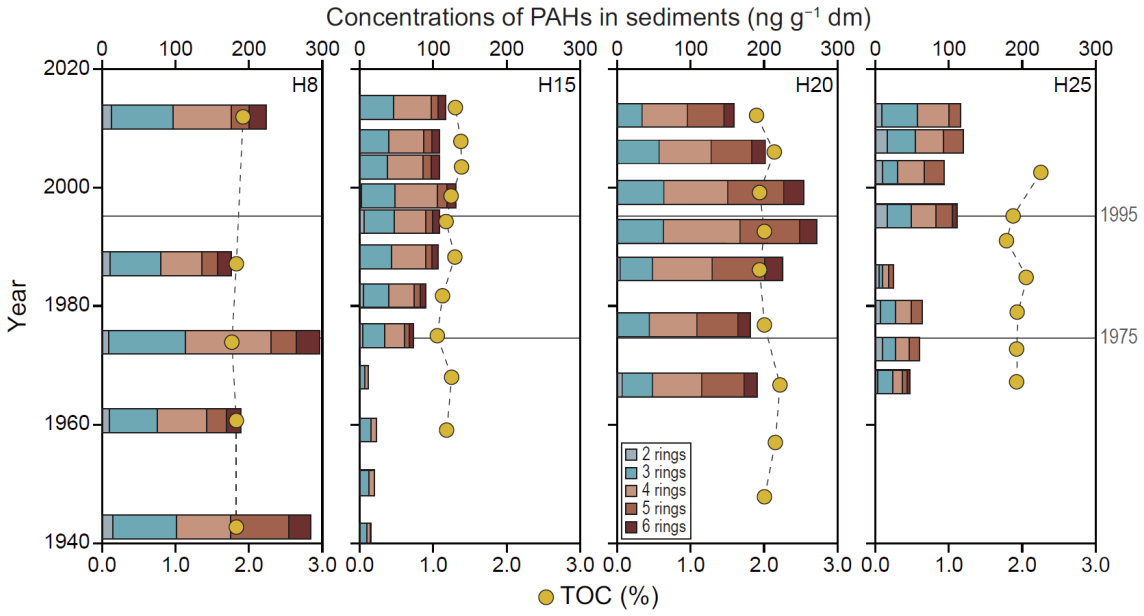

Fig. S7. Vertical distribution of PAHs and TOC in core sediments from four sites (H8, H15, H20, and H25) in the Hupo Basin. Sediment cores are divided into three time periods: 1940–1975, 1975–1995, 1995–present. Stacked bars represent the concentrations of PAHs categorized by ring number (2–6 rings), and yellow circles indicate TOC (%) at each depth interval.

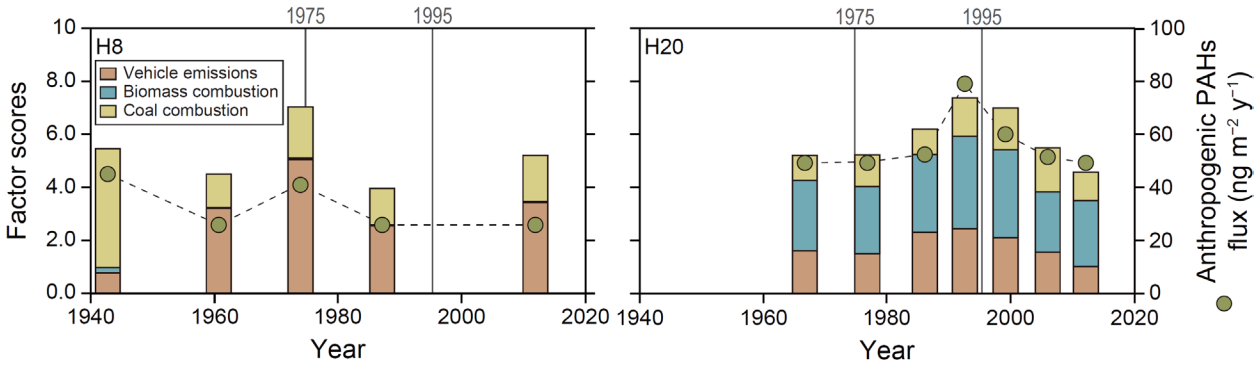

Fig. S8. Temporal variations in the relative contributions of PAH sources in core sediments from sites H8 and H20 in the Hupo Basin, as estimated by PMF modeling. Stacked bars represent the proportions of vehicle emissions, biomass combustion, and coal combustion. Green circles indicate anthropogenic PAH fluxes (ng m^{-2} yr^{-1}) at each sediment depth.

References

Durant, J.L., Busby Jr, W.F., Lafleur, A.L., Penman, B.W., Crespi, C.L., 1996. Human cell mutagenicity of oxygenated, nitrated and unsubstituted polycyclic aromatic hydrocarbons associated with urban aerosols. Mutat. Res.–Genet. Toxicol. 371, 123–157. https://doi.org/10.1016/S0165-1218(96)90103-2.

Durant, J.L., Lafleur, A.L., William, F.B.J., Lawrence, L.D., Bruce, W.P., Charles, L.C., 1999. Mutagenicity of C24H14 PAH in human cells expressing CYP1A1. Mutat. Res. 446, 1–14. https://doi.org/10.1016/S1383-5718(99)00135-7.

Lee, J.Y., Kim, Y.P., Kang, C.-H., Ghim, Y.S., Kaneyasu, N., 2006. Temporal trend and long-range transport of particulate polycyclic aromatic hydrocarbons at Gosan in northeast Asia between 2001 and 2004. J. Geophys. Res. Atmos. 111. https://doi.org/10.1029/2005JD006537.

Lee, S.C., Ho, K.F., Chan, L.Y., Zielinska, B., Chow, J.C., 2001. Polycyclic aromatic hydrocarbons (PAHs) and carbonyl compounds in urban atmosphere of Hong Kong. Atmos. Environ. 35, 5949–5960. https://doi.org/10.1016/S1352-2310(01)00374-0.

Nisbet, C., Lagoy, P., 1992. Toxic equivalency factors (TEFs) for polycyclic aromatic hydrocarbons (PAHs). Regul. Toxicol. Pharmacol. 16, 290–300. https://doi.org/10.1016/0273-2300(92)90009-X.

US EPA, 1993. Privisional guidance for quantitative risk assessment of Polycyclic Aromatic Hydrocarbons, US Environmental Protection Agency. Research Triangle Park, NC, EPA-600/R-93/089.